NACA RM H57H09

NACA

RESEARCH MEMORANDUM

FLIGHT DATA PERTINENT TO BUFFETING AND MAXIMUM NORMAL-FORCE COEFFICIENT OF THE DOUGLAS X-3 RESEARCH AIRPLANE

By Thomas F. Baker, James A. Martin, and Betty J. Scott

High-Speed Flight Station
Edwards, Calif.

NATIONAL ADVISORY COMMITTEE
FOR AERONAUTICS

WASHINGTON

November 20, 1957
Declassified July 17, 1958

NACA RM H57H09

NATIONAL ADVISORY COMMITTEE FOR AERONAUTICS

RESEARCH MEMORANDUM

FLIGHT DATA PERTINENT TO BUFFETING AND MAXIMUM NORMAL-FORCE COEFFICIENT OF THE DOUGLAS X-3 RESEARCH AIRPLANE

By Thomas F. Baker, James A. Martin, and Betty J. Scott

SUMMARY

The X-3 airplane, which has a straight 4.5-percent-thick wing of modified hexagonal section, has been flown to maximum wing normal-force coefficients in the Mach number range from 0.7 to 1.1 at an average altitude of 30,000 feet. Measurements were made of airplane and wing-panel maximum normal-force coefficients and of some buffeting characteristics. Limited data on the effects of a nominal 7° deflection of wing leading-edge flaps on the maximum lift and buffeting characteristics at subsonic speed were also obtained.

Airplane maximum normal-force coefficient was 0.65 in the Mach number range from 0.7 to 0.85, but thereafter increased rapidly with Mach number and reached a value on the order of 1.0 at a Mach number of 0.93. Wing-panel maximum normal-force coefficient decreased from 0.65 at a Mach number of 0.7 to 0.60 at a Mach number of approximately 0.8, but thereafter increased with Mach number (abruptly between Mach numbers of 0.9 and 0.95) and reached a value on the order of 1.3 at a Mach number of 1.05. Maximum wing lift defined the effective longitudinal maneuverability limit of the airplane throughout its speed range. High-altitude flight was precluded and moderate-altitude flight was severely limited at subsonic speeds by the combined effects of high wing loading and low maximum wing lift.

Buffeting occurred at a wing-panel normal-force coefficient about 0.2 below wing-panel maximum normal-force coefficient at Mach numbers up to 0.93 and at about 0.1 below wing-panel maximum normal-force coefficient at Mach numbers above 0.95. A rapid increase, rather than decrease, in the buffet boundary with Mach number in the Mach number range from 0.85 to 0.95 resulted from the elimination of shock-induced flow separation by use of the thin, low-aspect-ratio wing. The magnitude of the buffeting encountered did not constitute either an operational or a structural problem. Buffet-induced fluctuations in normal acceleration at the center

of gravity did not exceed ±0.3g below maximum lift at subsonic speeds. At supersonic speeds, the acceleration fluctuations were of negligible amplitude.

Deflecting the wing leading-edge flaps 7° in the Mach number range from 0.70 to 0.85 resulted in no appreciable change in wing-panel or airplane lift-curve slopes, but increased the values of maximum normal-force coefficient about 0.1 at Mach numbers below 0.8. The buffet boundary was raised by the 7° flap deflection to a normal-force coefficient about 0.15 above the clean-configuration boundary in the Mach number range from 0.70 to 0.85.

INTRODUCTION

The Douglas X-3 airplane is one of a series of research airplanes constructed for use by the National Advisory Committee for Aeronautics as part of the joint Air Force-Navy-NACA research program. The airplane was designed for sustained flight at supersonic speeds and has a straight, 4.5-percent-thick wing, and a long pointed fuselage which is large in comparison to the size of the wing. It is powered by two turbojet-afterburner combinations.

The transonic lift and buffeting characteristics of the X-3 airplane are of interest because of the somewhat unusual configuration of the airplane and particularly because of its thin, low-aspect-ratio wing which has a modified hexagonal airfoil and a leading-edge flap. The effects of airfoil thickness on transonic flow separation and buffeting have been studied in numerous investigations such as references 1 to 4. These investigations have shown that substantial alleviation of buffeting at transonic speeds should be obtainable through reduction in wing thickness ratio. In addition, the use of camber or leading-edge flaps to delay leading-edge-flow separation (refs. 4 to 6) would be expected to increase the buffet-free lift range of thin wings at subsonic speeds.

This paper presents the wing and airplane maximum lift and buffeting characteristics which were obtained during flight tests of the airplane by the NACA High-Speed Flight Station at Edwards, Calif. Limited data on the effects of a nominal 7° deflection of the leading-edge flaps on the lift and buffeting characteristics at subsonic speeds are included.

SYMBOLS

b	wing span
C_N	normal-force coefficient
C_{N_A}	airplane normal-force coefficient, nW/qS
C_{N_w}	wing-panel normal-force coefficient, N_w/qS_w
c	wing chord
g	acceleration due to gravity, ft/sec^2
h_p	pressure altitude, ft
i_t	stabilizer deflection with respect to fuselage reference line, positive when leading edge of stabilizer is up, deg
M	free-stream Mach number
N_w	aerodynamic normal force on wing panel, lb
n	normal-load factor, g units
q	free-stream dynamic pressure, lb/sq ft
S	total wing area, 166.5 sq ft
S_w	wing-panel area outboard of strain-gage station, (each side, 47.57 sq ft)
t	time, sec
W	airplane weight, lb
α	angle of attack, deg
Δa_n	incremental fluctuation of normal acceleration at center of gravity due to buffeting, ±g units
$\delta_{f_{le}}$	leading-edge-flap deflection, deg
$\dot{\theta}$	pitching angular velocity, radians/sec

Subscripts:

max	maximum
L	left
R	right

AIRPLANE

The Douglas X-3 airplane is a single-place straight-wing airplane powered by two J34 turbojet engines equipped with afterburners. The airplane is characterized by a long pointed fuselage which has appreciable projected plan-form area as compared to exposed wing area. A photograph of the airplane is shown in figure 1, and a three-view drawing is presented in figure 2(a). The physical characteristics and dimensions of the airplane are given in table I.

The wing is unswept at the 75-percent-chord line, is equipped with both leading- and trailing-edge flaps, and is mounted with zero incidence and dihedral. The wing section is a 4.5-percent-thick hexagonal airfoil, modified by rounding the corners. A section view of the wing at midsemispan is shown in figure 2(b). The airplane has an all-movable horizontal-tail surface and conventional flap-type rudder and aileron control surfaces. All the aerodynamic control surfaces are powered by an irreversible hydraulic system and have variable artificial force gradients.

The wing is constructed of heavy tapered aluminum-alloy plating, separated by a multicellular core. The fuselage is of semimonocoque construction consisting of closely spaced frames, a relatively small number of longerons, and comparatively heavy skin. The horizontal tail is constructed of titanium skin stiffened by chordwise ribs. Each side of the horizontal tail is assembled on one double-webbed steel spar which terminates as a combined spar and torque tube. The vertical tail has a main spar, rudder support spar, and heavy skin stiffened by chordwise ribs.

INSTRUMENTATION

The X-3 airplane was equipped with standard NACA recording instruments for measuring the following quantities pertinent to this investigation:

Airspeed
Altitude

Angles of attack and sideslip
Control surface positions
Three components of acceleration
Angular velocities
Structural loads and stresses
Left-wing surface pressures

The airspeed head and angle-of-attack vane were mounted on a boom projecting from the nose of the airplane. Strain gages were installed at the roots of both wing panels, on the vertical tail, and on both sides of the horizontal stabilizer as shown in figure 2(a). The bending bridges were cemented either to spar caps or to the skin inner surfaces. The shear bridges were cemented to spar or core webs. A fluid-damped Statham accelerometer, maintained at a constant temperature by a thermostatically controlled heating jacket, was installed near the airplane center of gravity to measure fluctuations in normal acceleration during buffeting. The strain gages and Statham accelerometer were recorded on a 36-channel Consolidated recording oscillograph with dynamic response flat (within ±5 percent) to about 60 cycles per second. All instruments were synchronized by a common timer.

The airspeed system was calibrated by using the radar-phototheodolite method of reference 7. The values presented herein for angle of attack were not corrected for the effects of upwash, boom bending, or pitching velocity. Both strain-gage and pressure measurements were used to determine values of wing-panel normal-force coefficient C_{N_w}; strain-gage results for the flap-undeflected configuration, and left-wing-surface pressure measurements (ref. 8) for the flap-deflected configuration. The two methods gave equally good measures of wing-panel aerodynamic characteristics for the flap-undeflected configuration. The strain gages were calibrated by applying static loads to the structure. The wing strain-gage calibration applied only to the flap-undeflected configuration and was not accurate for the flap-deflected configuration.

The estimated overall accuracies of the salient quantities presented in this paper are:

M	±0.01
C_{N_A}	±0.01
C_{N_w}	±0.04
α, deg	±1.0

RESULTS AND DISCUSSION

Maximum Normal-Force Coefficients

General characteristics.- Typical variations with angle of attack of airplane normal-force coefficient C_{N_A}, wing-panel normal-force coefficient C_{N_w}, stabilizer position, and pitching velocity are presented in figure 3 for several Mach numbers to show the general characteristics of pertinent quantities during longitudinal maneuvers. All data presented in this paper were obtained during low pitching rate accelerated turns and push-down pull-up maneuvers at altitudes varying from 28,000 to 35,000 feet in the Mach number range from 0.7 to 1.15. The variation of C_{N_A} and C_{N_w} with angle of attack is characterized by an essentially linear variation up to moderate angles of attack followed by a generally gradual reduction in slope to maximum wing lift. The initial reduction in wing lift-curve slope has been termed the wing "lift break." Wing and airplane maximum normal-force coefficients are defined as the values of C_{N_w} and C_{N_A} at which $dC_{N_w}/d\alpha$ and $dC_{N_A}/d\alpha$ are essentially zero. It should be noted that airplane maximum normal-force coefficients were not attained at Mach numbers above 0.93, although, as shown in figures 3(e) and 3(f), $dC_{N_A}/d\alpha$ continuously decreased above an angle of attack of about 12°. Mild pitch-ups, sometimes accompanied by a roll-off, occurred throughout the speed range as maximum lift was approached. The pitch rate during the pitch-up was generally low (less than 0.3 radian/sec).

Maximum lift boundaries.- The lift data obtained during the tests are summarized in figures 4 to 6. It may be seen that wing-panel maximum normal-force coefficient decreased from 0.65 at a Mach number of 0.7 to 0.60 at a Mach number of approximately 0.8, but thereafter increased with Mach number (abruptly between Mach numbers of 0.90 and 0.95), and reached a value on the order of 1.3 at a Mach number of 1.05. It is interesting to note that at low supersonic speed, the values of $C_{N_{w_{max}}}$ and the corresponding angles of attack were almost twice the values at subsonic speed ($M \approx 0.8$). The airplane normal-force-coefficient data (fig. 6) show the same trend with Mach number as the wing-panel data of figure 4, except below $M \approx 0.85$ the values of $C_{N_{A_{max}}}$ were essentially constant at 0.65. Maximum airplane normal-force coefficient was 1.0 at $M = 0.93$. At Mach numbers above 0.93, maximum values of airplane normal-force coefficient were not attained even though angles of attack on the order of 18° were reached.

Some indication of the wing flow characteristics at maximum lift is provided by the pressure-distribution data of references 8 and 9 and

by the wind-tunnel investigations of references 10 and 11. In general, below a Mach number of about 0.94, the wing lift break and maximum lift are the result of wing upper surface flow separation. Above a Mach number of 0.94 the wing flow is essentially supersonic to maximum lift, and the lift break and maximum lift are primarily the result of the attainment of limit pressure over part of the upper surface.

Usable load factor.- The influence of the maximum lift boundary on flight operations conducted with this airplane is of interest. In figure 7 the variation of airplane normal-load factor for maximum wing lift is shown as a function of Mach number for several altitudes. The normal-load factor for maximum wing lift, rather than heavy buffeting or maximum airplane lift, defines the effective longitudinal maneuverability limit for this airplane because of the large increase in drag associated with wing stall, the decay in longitudinal stability, which at subsonic speeds is almost coincidental with $C_{N_{W_{max}}}$ and, as shown in the following section, the absence of all but incipient buffeting below maximum wing lift. It may be seen in figure 7 that at subsonic speeds, high-altitude flight was precluded and moderate-altitude flight was severely limited by the combined effects of high wing loading (W/S = 120) and low maximum wing lift.

Buffeting

General characteristics.- Three typical oscillograph records of wing, horizontal-tail, and vertical-tail strain-gage responses are reproduced in figure 8. The strain-gage locations and oscillograph channel identification are given in table II. The start of wing buffeting (indicated on each record by an arrow) was evidenced by the occurrence of wing bending-stress fluctuations. The onset of tail buffeting was evidenced by fluctuations in the outputs of both tail shear and tail bending gages. Wing bending-stress fluctuations were recorded at about 16 cycles per second and wing shear-stress fluctuations at about 45 cycles per second. Shear and bending stresses in the vertical tail fluctuated at about 30 cycles per second. Horizontal-tail bending stresses were recorded at about 25 cycles per second and the horizontal-tail shear stresses fluctuated at 25 cycles per second and at about 70 cycles per second. The natural structural modes of vibration to which the buffet frequencies appeared to correspond were:

Wing bending stresses	1st symmetrical wing bending
Wing shear stresses	1st symmetrical wing torsion
Vertical-tail stresses	1st vertical-tail bending

Horizontal-tail bending stresses	1st symmetrical horizontal-tail bending
Horizontal-tail shear stresses	Unsymmetrical horizontal-tail torsion

Buffet boundaries.- The wing buffet boundary, which defines the buffet boundary for the airplane, and the wing buffet-intensity rise, which denotes the first apparent increase in buffet intensity as penetration into the buffet region increases, are presented as functions of wing-panel normal-force coefficient and Mach number in figure 9; as functions of airplane normal-force coefficient and Mach number in figure 10; and as functions of angle of attack and Mach number in figure 11. It may be seen that the buffet boundary and the maximum lift boundary exhibit the same variation with Mach number. Buffeting occurred at a normal-force coefficient about 0.2 below maximum lift at Mach numbers up to 0.93, and at about 0.1 below maximum lift at Mach numbers above 0.95. The abrupt increase, rather than decrease, in the buffet boundary as Mach number is increased from about 0.85 to 0.95 results from the elimination of shock-induced wing flow separation, and was achieved by use of a thin, low-aspect-ratio wing. The start of horizontal-tail buffeting may be seen in figures 10 and 11 to be coincidental with the wing buffet-intensity rise at Mach numbers below 0.90, while at Mach numbers above 0.95, tail buffeting was coincidental with the start of wing buffeting.

It is generally recognized that low-lift transonic buffeting results from shock-induced wing flow separation. Reduction in wing thickness and, to some extent, aspect ratio, decreases the strength of the wing shock. For wings with thickness ratios less than about 0.06, the shock is not strong enough to separate the boundary layer at low lifts, thus eliminating low-lift transonic buffeting for such thin wings. Shock strength increases with angle of attack and the onset of buffeting at moderate lift at a Mach number of about 0.85 is the result of shock-induced separation over the rearward part of the wing. The upturn in the buffet boundary as Mach number is increased from 0.85 to 0.95 results from the opposing effects of angle of attack and Mach number on shock position - as Mach number increases, the shock tends to move toward the trailing edge, and as angle of attack increases, the shock tends to move toward the leading edge. It is probable that in this Mach number range, the buffet boundary approximates a curve for a constant shock position.

Wing flow characteristics.- The occurrence of leading-edge flow separation at the wing root, midsemispan, and tip orifice stations (from ref. 8) is compared with the buffet boundary in figure 12. Also shown is the variation with angle of attack of the critical Mach number at three spanwise wing stations (from ref. 10). There is little correlation between leading-edge separation and buffeting with the exception of the transonic increase with Mach number of both the buffet boundary and the

separation boundaries. Correlation between critical Mach number and buffeting is nonexistent as would be expected for a wing of thin airfoil section.

The lack of correlation between leading-edge separation and buffeting is understandable when it is realized that the leading-edge-separation boundaries of reference 8 define only the occurrence of separated flow indicated by the pressure orifices closest to the leading edge and connote nothing about the flow conditions aft of the leading edge. Determination of the flow conditions aft of the leading edge from presently available flight measurements (ref. 9) was not possible because of limited transonic Mach number coverage. However, the wind-tunnel results of references 10 and 11 do provide the following gross picture of the wing flow characteristics: At a Mach number of 0.6, the leading-edge separation is initially confined to about the forward 10-percent chord and as angle of attack is increased, the flow reattachment point moves rearward until complete upper-surface stall occurs; at a Mach number of 0.8, similar flow conditions prevail except that at midsemispan the flow reseparates at about 35-percent chord after initial leading-edge separation and reattachment, and increase in angle of attack results in an increase in the leading edge and midchord separation areas; at Mach numbers of 0.90 and 0.925, separation occurs first over the trailing edge of the wing and progresses toward the leading edge as angle of attack is increased.

The relation between flow separation and the onset of buffeting can be described as follows. At Mach numbers below about 0.8, flow separation occurs at the leading edge but initially exists over only a small area along the leading edge; the random force generated by the fluctuating pressures acting over this small area is not sufficient to excite vibratory motion of the wing. As angle of attack is increased, the magnitude of the random force is increased due to the increase in surface area over which separation exists (and the pressure fluctuations act), and wing vibration (buffeting) results. As Mach number is increased from about 0.8, the flow-separation pattern changes from separation at the leading edge progressing rearward with angle of attack, to separation at both the leading and the trailing edge progressing toward the quarter chord from both directions with angle of attack to separation at the trailing edge progressing forward with angle of attack. The onset of buffeting at angles of attack below the occurrence of leading-edge separation (Mach numbers above about 0.8) thus appears to be the result of separation over the rearward area of the wing. Above a Mach number of about 0.85, the leading-edge-separation boundaries are indicative of almost complete wing stall.

The occurrence of supersonic buffeting at Mach numbers above 0.95 probably results from the occurrence of a small region of separated flow along the trailing edge of the wing at high angles of attack.

Buffet magnitude.- The magnitude of the buffeting encountered by this airplane below maximum lift did not constitute an operational or a structural problem and imposed no limitation on operation of the airplane. The buffet-induced wing stresses were less than 2 percent of "design load stress" below airplane maximum normal-force coefficient, and buffet-induced stresses in the horizontal tail were less than 5 percent of design load stress below airplane maximum normal-force coefficient. Design load stress is defined as the maximum stress developed by application of design limit loads during static tests. During one maneuver, however, which went well beyond the stall (figs. 3(d) and 8(b)), the wing buffet stresses reached values on the order of 3.5 percent, and the horizontal- and vertical-tail stresses reached values on the order of 10 percent of design load stress.

Results of measurements of fluctuations in normal acceleration at the center of gravity at a nominal altitude of 30,000 feet are shown in figure 13. It may be seen that at subsonic speeds the values of Δa_n did not exceed $\pm 0.3g$ below maximum wing lift. At supersonic speeds the magnitude of the buffeting was negligible. The acceleration fluctuations occurred at a frequency of about 16 cycles per second with a higher frequency on the order of 60 to 70 cycles per second superimposed on the lower frequency. The 16-cycle-per-second vibration corresponds approximately to the first mode of symmetrical wing bending.

Stall warning.- Buffeting did not provide adequate warning of pitch-up or maximum lift for this airplane. At Mach numbers below 0.9, the lift range between the onset of buffeting and maximum lift was too large, and the increase of buffet magnitude with lift was too small to provide a usable warning to the pilot of imminent pitch-up or stall. Conversely, at Mach numbers between about 0.90 and 0.95, the lift and speed range between the buffet boundary and maximum lift was too small to provide adequate warning. At supersonic speeds, the buffeting could barely be detected by the pilot but was used, in conjunction with increasing stick force and normal acceleration, to indicate that maximum lift was being approached. For all practical purposes, however, the pilot believed that stall warning was nonexistent at supersonic speeds.

Effects of Leading-Edge-Flap Deflection

Effect on lift.- Several exploratory longitudinal maneuvers with leading-edge flaps deflected a nominal 7° were made at Mach numbers between 0.7 and 0.9. It should be noted that the nominal 7° deflection tested was not necessarily the optimum for minimum drag, maximum lift, buffet alleviation, etc., and that flap deflection during the maneuvers was not constant but gradually decreased from about 9° at zero lift to about 6° at peak lift as the leading-edge loading increased. The

variation with angle of attack of airplane and wing-panel normal-force coefficients for the flap-deflected configuration is shown in figure 14 for several Mach numbers. The effects of the flap deflection on maximum lift are summarized in figure 15 as a function of Mach number. Deflection of the leading-edge flaps resulted in no appreciable change in wing-panel or airplane lift-curve slopes; however, as seen from figure 15, maximum normal-force coefficients were increased on the order of 0.1 by the 7° flap deflection. This increase in maximum normal-force coefficient is a result of the camber effect derived by drooping the leading edge, which delays separation to a higher angle of attack. Maximum normal-force coefficients were not attained at Mach numbers above 0.8 in the flap-deflected configuration as a result of termination of the maneuvers by the pilot because of imminent pitch-up or lateral instability (roll-off). The peak values of C_{N_A} shown in figure 15 thus tend to represent the maximum usable lift for the flap-deflected configuration investigated.

The necessity for increasing wing maximum lift at subsonic speeds was shown by the variation of airplane normal-load factor with Mach number for various altitudes in figure 7. The utilization of leading-edge flaps as a means of increasing subsonic maximum lift is shown in figure 14 to be quite effective, and although the data were obtained for only one flap position over a limited Mach number range, the flight results confirm the results obtained in wind-tunnel studies such as reference 12, and in wind-tunnel tests of the X-3 model (refs. 10 and 11). These investigations have shown that at transonic and subsonic speeds, deflection of a leading-edge flap results in a rearrangement of the wing pressure distribution that, at low and moderate angles of attack, causes little change in net lift and a rearward shift in the center of pressure, but which at moderate and high angles of attack achieves substantial reductions in drag and substantial increases in maximum lift and lift-drag ratios.

Determination of optimum flap positions for cruise, longitudinal maneuvers, maximum lift, and maximum lift-drag ratio was not possible during the present tests, but analysis of wind-tunnel data such as reference 12 clearly shows that the optimum flap positions for each of the foregoing flight operations are different and that optimum flap position for any operation varies with Mach number and angle of attack. Manual operation or pre-set sequencing to a fixed position of leading-edge flaps achieves some beneficial effects for some operations, such as cruising flight, but also has certain disadvantages. For instance, during the present tests, the flaps were deflected from level, trimmed flight at the rate of about 3 degrees per second. An abrupt, disconcerting, nose-down trim change, termed by the pilot as "excessive," occurred as a result of the rearward shift of the center of pressure. In addition, deflection of a leading-edge flap at low angles of attack results in

increased drag and, in some cases, buffeting, when the lower surface of the flap is at a negative angle of attack. It thus appears that in order to obtain optimum results from a leading-edge flap, automatic positioning of the flap as a function of Mach number and angle of attack is required.

Effects on buffeting.- The buffet-boundary characteristics of the airplane in the flap-deflected configuration are shown in figure 16. Comparison of the wing buffet boundary for the flap-deflected configuration with the wing buffet boundary for the clean configuration is shown in figure 17. The values of C_{N_A} for the onset of wing buffet, which define the airplane buffet boundary, were increased approximately 0.15 by the 7° flap deflection for Mach numbers from 0.7 to 0.8. The values of C_{N_A} at which the wing buffet-intensity rise occurred were increased approximately 0.2 over this same Mach number range. The onset of tail buffet was slightly before, or coincident with the wing buffet-intensity rise, as was the case with the flaps undeflected. The leading-edge flaps gradually lose their effectiveness as buffet alleviators as Mach number is increased from 0.85 to 0.90. At Mach numbers above 0.85, buffeting is predominantly the result of shock-induced flow separation over the rearward part of the wing and small deflections of a leading-edge flap would be expected to be ineffective in delaying or reducing such separation. Larger deflections of a leading-edge flap would result in earlier flow separation on the upper surface and probably cause flow separation on the lower surface.

CONCLUDING REMARKS

Measurements were made of airplane and wing-panel maximum lift and buffeting characteristics of the Douglas X-3 airplane in the Mach number range from 0.7 to 1.1. Airplane maximum normal-force coefficient was 0.65 in the Mach number range from 0.7 to 0.85, but thereafter increased rapidly with Mach number and reached a value on the order of 1.0 at a Mach number of 0.93. Wing-panel maximum normal-force coefficient decreased from 0.65 at a Mach number of 0.7 to 0.60 at a Mach number of approximately 0.8, but thereafter increased with Mach number (abruptly between Mach numbers of 0.9 and 0.95) and reached a value on the order of 1.3 at a Mach number of 1.05. Maximum wing lift defined the effective longitudinal maneuverability limit of the airplane throughout its speed range. High-altitude flight was precluded and moderate-altitude flight was severely limited at subsonic speeds by the combined effects of high wing loading and low maximum wing lift.

Buffeting occurred at a wing-panel normal-force coefficient about 0.2 below wing-panel maximum normal-force coefficient at Mach numbers up

to 0.93 and at about 0.1 below wing-panel maximum normal-force coefficient at Mach numbers above 0.95. A rapid increase, rather than decrease, in the buffet boundary with Mach number in the Mach number range from 0.85 to 0.95 resulted from the elimination of shock-induced flow separation by use of the thin, low-aspect-ratio wing. The magnitude of the buffeting encountered did not constitute either an operational or a structural problem. Buffet-induced fluctuations in normal acceleration at the center of gravity did not exceed ±0.3g below maximum lift at subsonic speeds. At supersonic speeds, the acceleration fluctuations were of negligible amplitude.

Deflecting the wing leading-edge flaps a nominal 7° in the Mach number range from 0.7 to 0.85 resulted in no appreciable change in wing-panel or airplane lift-curve slopes, but increased the values of maximum normal-force coefficient about 0.1 at Mach numbers below 0.8. The buffet boundary was raised by the 7° flap deflection to a normal-force coefficient about 0.15 above the clean-configuration boundary in the Mach number range from 0.70 to 0.85.

High-Speed Flight Station,
National Advisory Committee for Aeronautics,
Edwards, Calif., July 30, 1957.

REFERENCES

1. Purser, Paul E., and Wyss, John A.: Review of Some Recent Data on Buffet Boundaries. NACA RM L51E02a, 1951.

2. Humphreys, Milton D.: Pressure Pulsations on Rigid Airfoils at Transonic Speeds. NACA RM L51I12, 1951.

3. Coe, Charles F., and Mellenthin, Jack A.: Buffeting Forces on Two-Dimensional Airfoils as Affected by Thickness and Thickness Distribution. NACA RM A53K24, 1954.

4. Polentz, Perry P., Page, William A., and Levy, Lionel L., Jr.: The Unsteady Normal-Force Characteristics of Selected NACA Profiles at High Subsonic Mach Numbers. NACA RM A55C02, 1955.

5. Humphreys, Milton D., and Kent, John D.: The Effects of Camber and Leading-Edge-Flap Deflection on the Pressure Pulsations on Thin Rigid Airfoils at Transonic Speeds. NACA RM L52G22, 1952.

6. Humphreys, Milton D.: Transonic Aerodynamic Characteristics of an NACA 64A006 Airfoil Section With a 15-Percent-Chord Leading-Edge Flap. NACA RM L53G23, 1953.

7. Zalovcik, John A.: A Radar Method of Calibrating Airspeed Installations on Airplanes in Maneuvers at High Altitudes and at Transonic and Supersonic Speeds. NACA Rep. 985, 1950. (Supersedes NACA TN 1979.)

8. Keener, Earl R., and Jordan, Gareth H.: Wing Loads and Load Distributions Throughout the Lift Range of the Douglas X-3 Research Airplane at Transonic Speeds. NACA RM H56G13, 1956.

9. Jordan, Gareth H., and Hutchins, C. Kenneth, Jr.: Preliminary Flight-Determined Pressure Distributions Over the Wing of the Douglas X-3 Research Airplane at Subsonic and Transonic Mach Numbers. NACA RM H55A10, 1955.

10. Cleary, Joseph W., and Mellenthin, Jack A.: Wind-Tunnel Tests of a 0.16-Scale Model of the X-3 Airplane at High Subsonic Speeds. Wing and Fuselage Pressure Distribution. NACA RM A50D07, 1950.

11. Hamilton, William T., and Cleary, Joseph W.: Wind-Tunnel Tests of a 0.16-Scale Model of the X-3 Airplane at High Subsonic Speeds. Stability and Control Characteristics. NACA RM A50A03, 1950.

12. Johnson, Ben H., Jr., and Reed, Verlin D.: Investigation of a Thin Wing of Aspect Ratio 4 in the Ames 12-Foot Pressure Wind Tunnel. IV - The Effect of a Constant-Chord Leading-Edge Flap at High Subsonic Speeds. NACA RM A8K19, 1949.

TABLE I

PHYSICAL CHARACTERISTICS OF THE DOUGLAS X-3 AIRPLANE

Wing:	
Airfoil section	Modified hexagon
Airfoil thickness ratio, percent chord	4.5
Total area, sq ft	166.50
Wing-panel area (outboard of station 45) each side, sq ft	47.57
Span, ft	22.69
Mean aerodynamic chord, ft	7.84
Root chord, ft	10.58
Tip chord, ft	4.11
Taper ratio	0.39
Aspect ratio	3.09
Sweep at 0.75 chord line, deg	0
Incidence, deg	0
Dihedral, deg	0
Geometric twist, deg	0
Aileron area rearward of hinge line (each), sq ft	4.04
Aileron span at hinge line (each), ft	3.25
Aileron chord rearward of hinge line, percent wing chord	25
Aileron travel (each), deg	±12
Leading-edge flap:	
Type	Plain
Area (each), sq ft	8.38
Span at hinge line (each), ft	8.916
Chord, normal to hinge line, in.	11.50
Travel, deg	30
Trailing-edge flap:	
Type	Split
Area (each), sq ft	8.61
Span, ft	5.083
Chord, percent wing chord	25
Travel, deg	50
Horizontal tail:	
Airfoil section	Modified hexagon
Airfoil thickness ratio at root chord, percent chord	8.01
Airfoil thickness ratio outboard station 26, percent chord	4.50
Total area, sq ft	43.24
Span, ft	13.77
Mean aerodynamic chord, ft	3.34
Root chord, ft	4.475
Tip chord, ft	1.814
Taper ratio	0.405
Aspect ratio	4.38
Sweep at leading edge, deg	21.14
Sweep at trailing edge, deg	0
Dihedral, deg	0
Travel:	
Leading edge up, deg	6
Leading edge down, deg	17
Hinge-line location, percent root chord	46.46
Vertical tail:	
Airfoil section	Modified hexagon
Airfoil thickness ratio, percent chord	4.5
Area, sq ft	23.73
Span, (from horizontal-tail hinge line), ft	5.59
Mean aerodynamic chord, ft	4.69
Root chord, ft	6.508
Tip chord, ft	1.93
Taper ratio	0.292
Aspect ratio	1.515
Sweep at leading edge, deg	45
Sweep at trailing edge, deg	9.39
Rudder area, rearward of hinge line, sq ft	5.441
Rudder span at hinge line, ft	3.535
Rudder root chord, ft	1.98
Rudder tip chord, ft	1.097
Rudder travel, deg	±20
Fuselage:	
Length including boom, ft	66.75
Maximum width, ft	6.08
Maximum height, ft	4.81
Base area, sq ft	7.94
Powerplant:	
Engines	Two Westinghouse J34-WE-17 with afterburners
Rating, each engine:	
Static sea-level maximum thrust, lb	4,850
Static sea-level military thrust, lb	3,370
Airplane weight, lb:	
Take-off	22,050
Landing	17,000
Center-of-gravity location, percent mean aerodynamic chord:	
Take-off	4.7
Landing (gear up)	-1.5
Landing (gear down)	-0.8

TABLE II

OSCILLOGRAPH HOOKUP

Surface	Strain-gage location	Type	Oscillograph channel number	
			Figure 8(a) Figure 8(b)	Figure 8(c)
Right wing	32-percent chord	Shear	2	5
	50-percent chord	Shear	13	3
	68-percent chord	Shear	3	6
	46-percent chord	Bending	6	10
	54-percent chord	Bending	7	11
Left wing	32-percent chord	Shear	4	7
	50-percent chord	Shear	14	4
	68-percent chord	Shear	5	8
	46-percent chord	Bending	8	12
	54-percent chord	Bending	9	13
Right horizontal tail	Forward spar web	Shear	15	23
	Aft spar web	Shear	17	25
	Spar caps	Bending	19	30
Left horizontal tail	Forward spar web	Shear	16	24
	Aft spar web	Shear	18	26
	Spar caps	Bending	20	31
Vertical tail	Front spar web	Shear	27	17
	Rear spar web	Shear	28	18
	Front spar attachment fitting, bending	Bending	25	15
	Rear spar attachment fitting, bending	Bending	26	16
Airplane center of gravity	Statham accelerometer	Vertical	24	14

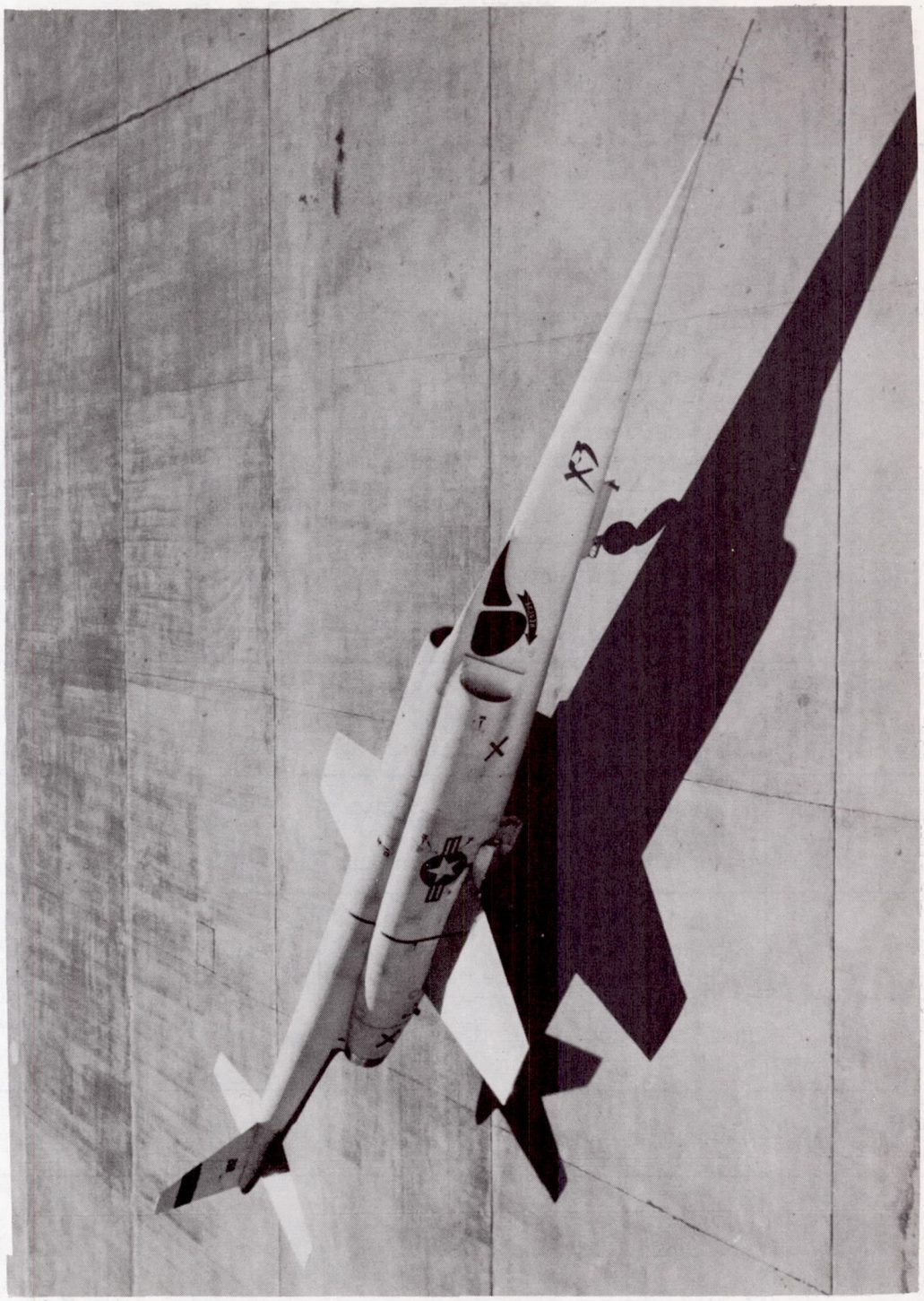
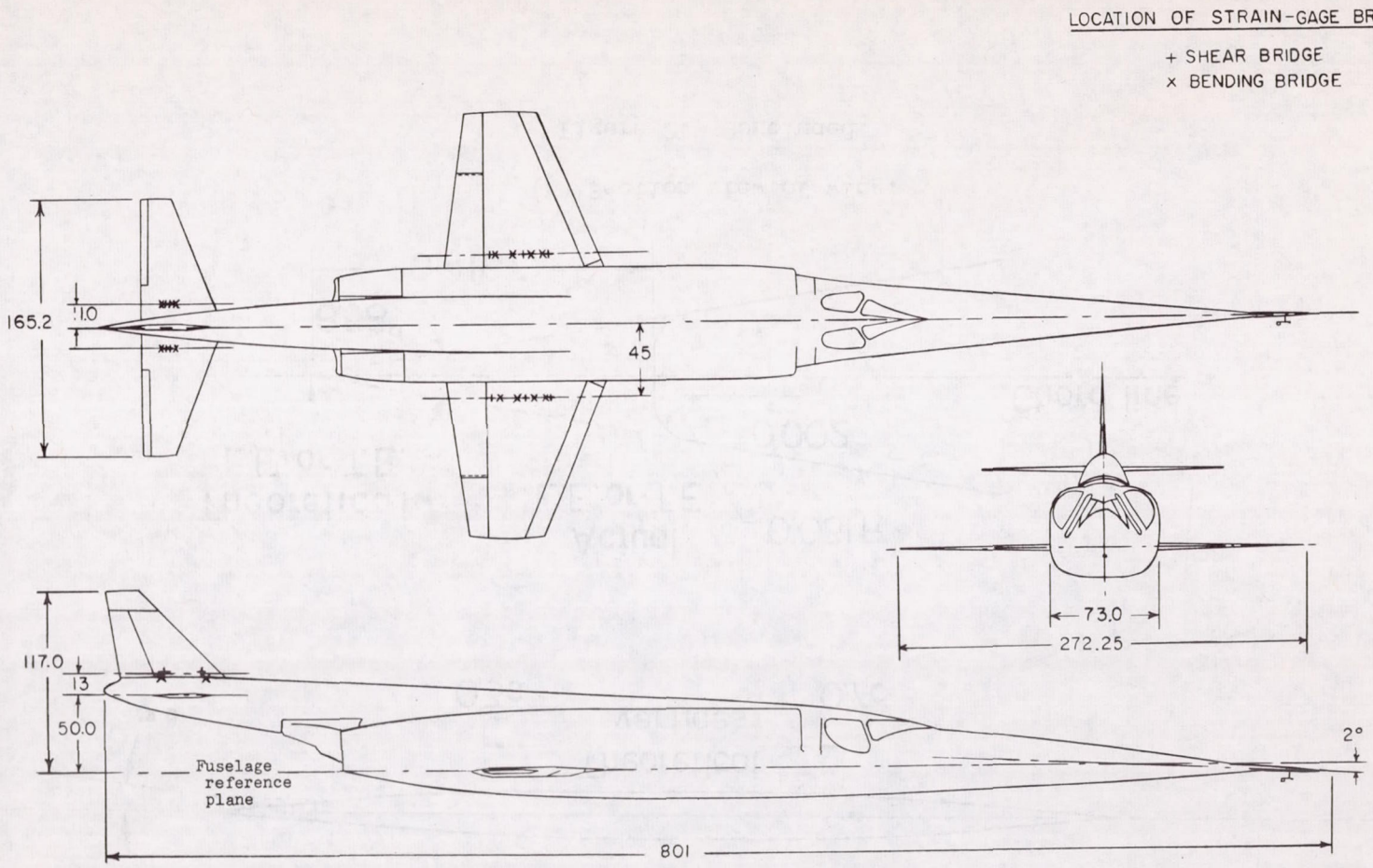
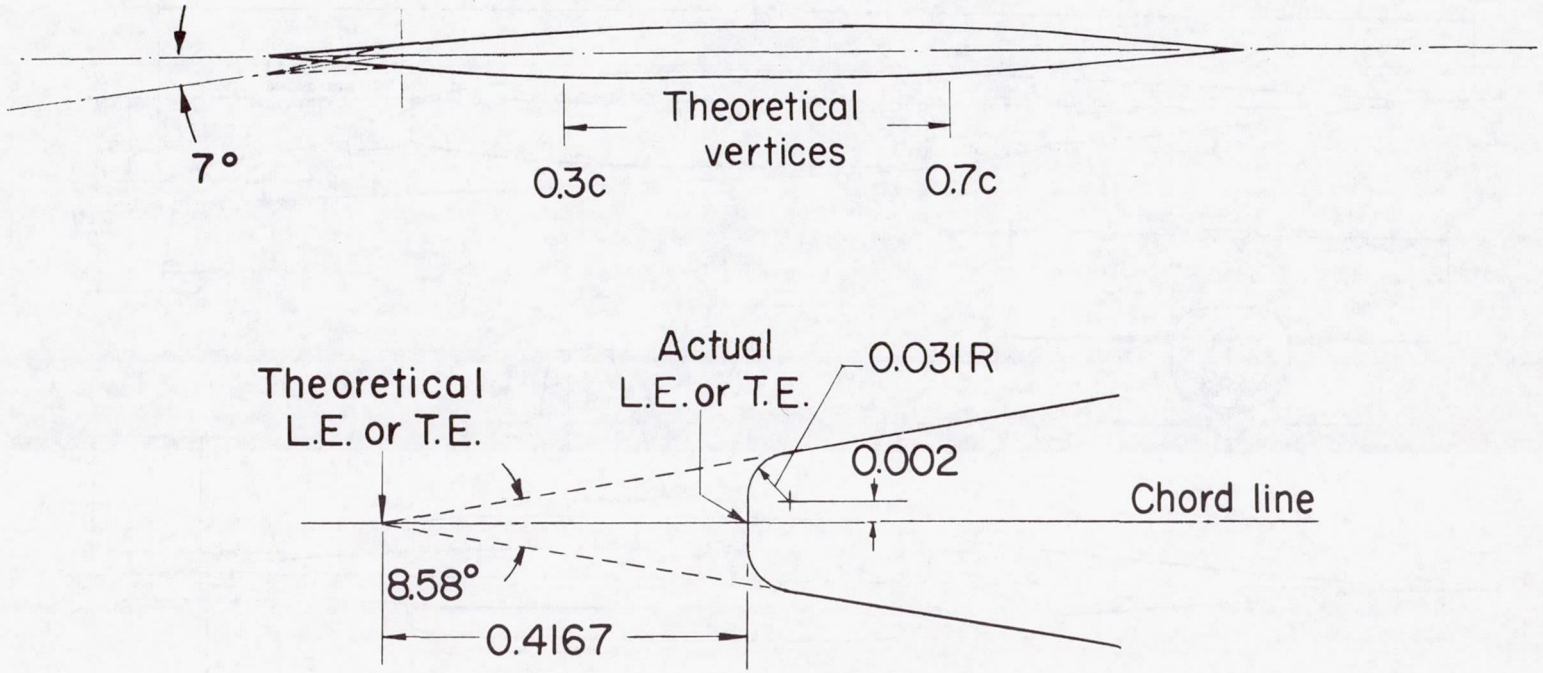


Figure 1.- Photograph of the Douglas X-3 research airplane. E-1995



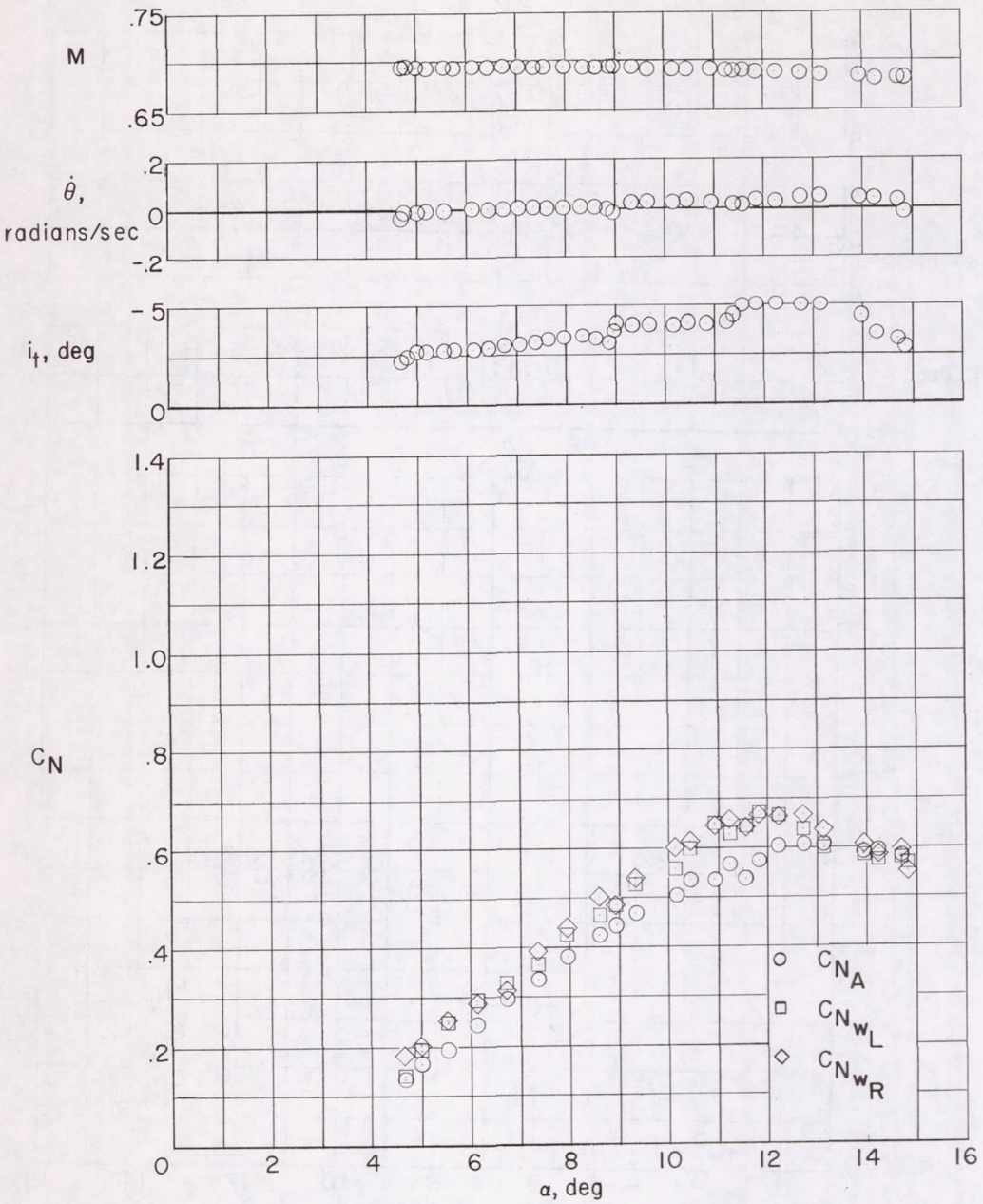
(a) Three-view drawing of airplane.

Figure 2.- Drawings of the X-3 research airplane. All dimensions in inches unless otherwise noted.



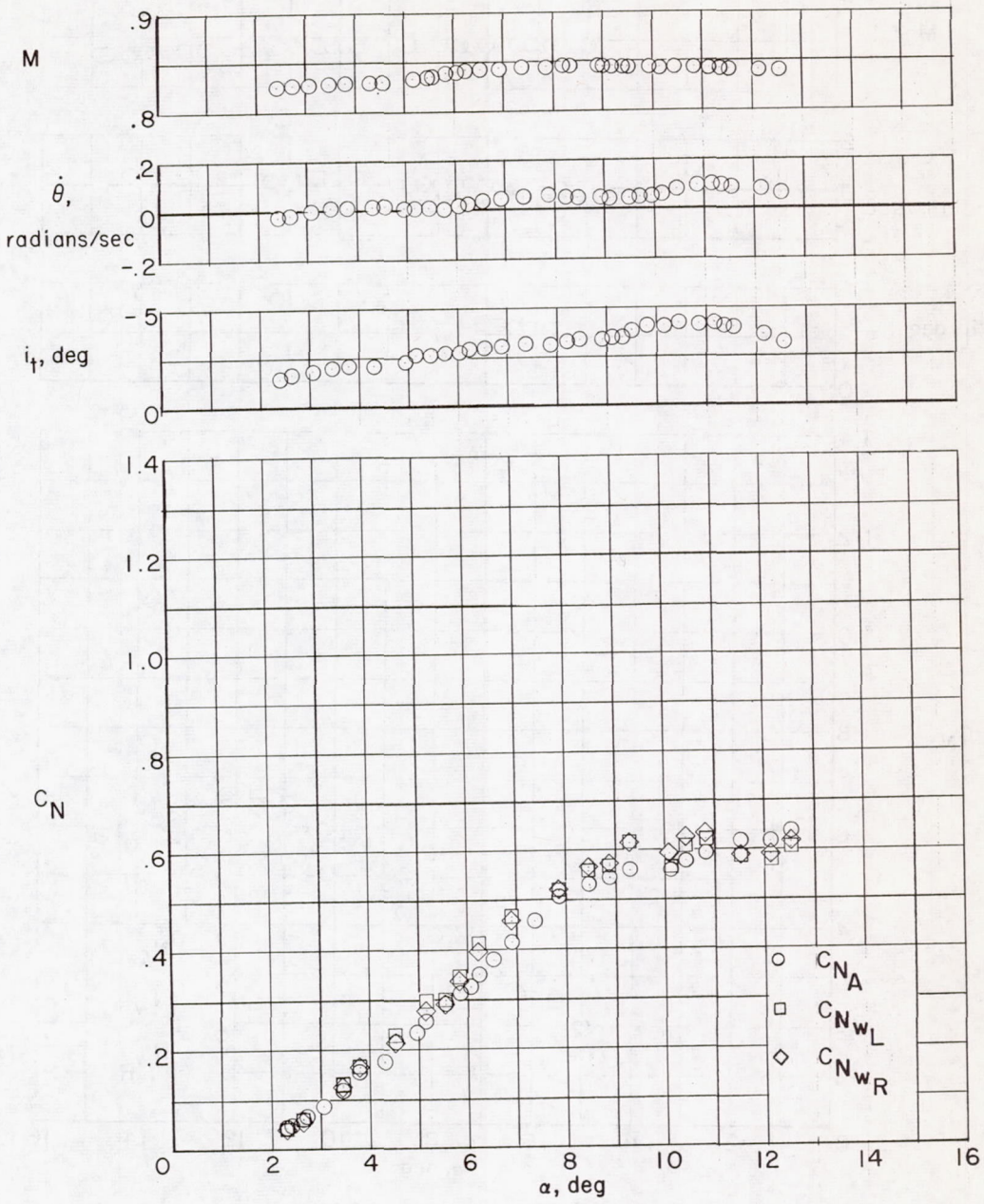
(b) Section view of wing.

Figure 2.- Concluded.



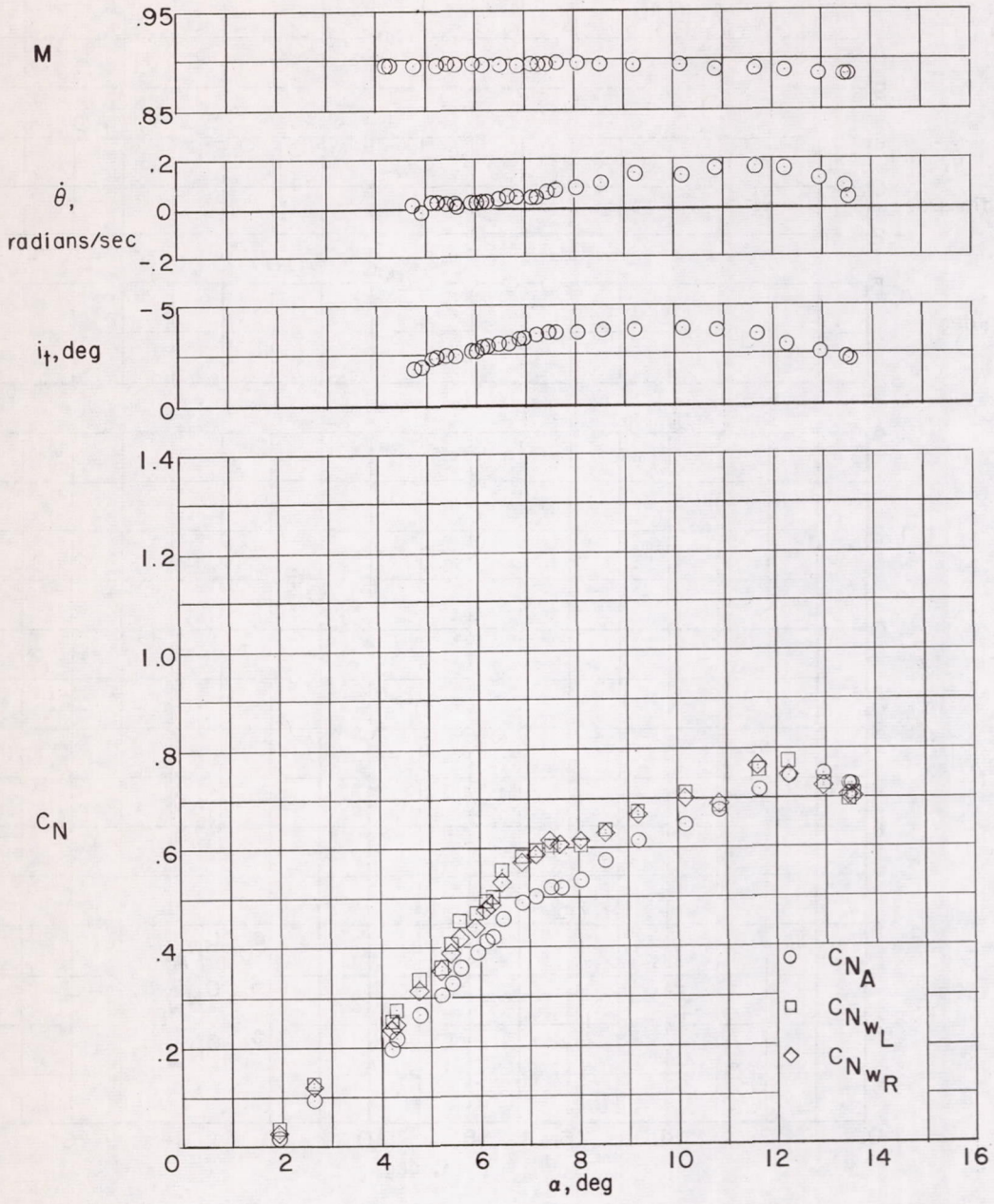
(a) $M \approx 0.70$; $h_p \approx 35{,}000$ feet.

Figure 3.- Variation of wing-panel and airplane normal-force coefficient with angle of attack during pull-up. X-3 airplane.



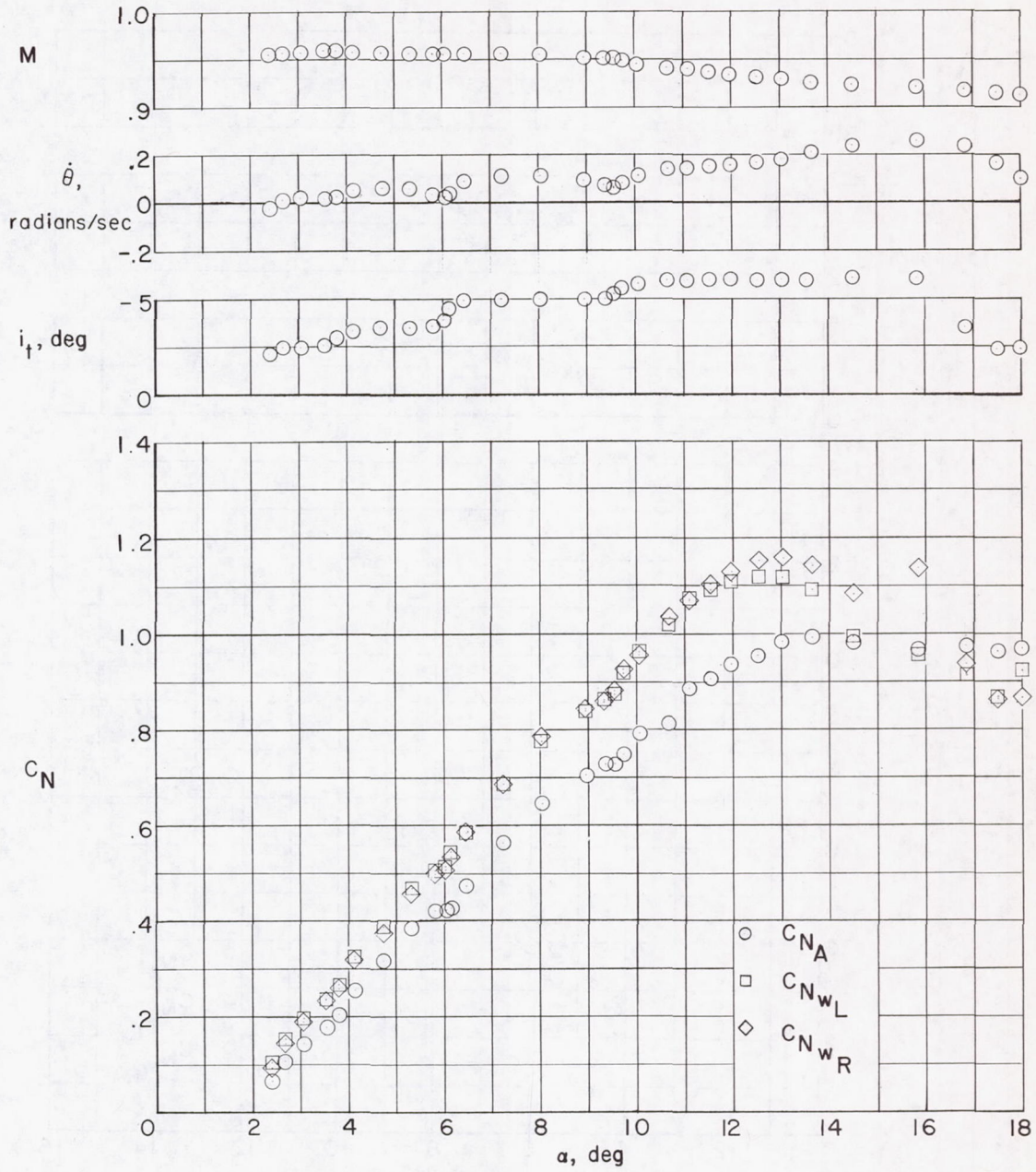
(b) $M \approx 0.84$; $h_p \approx 32{,}000$ feet.

Figure 3.- Continued.



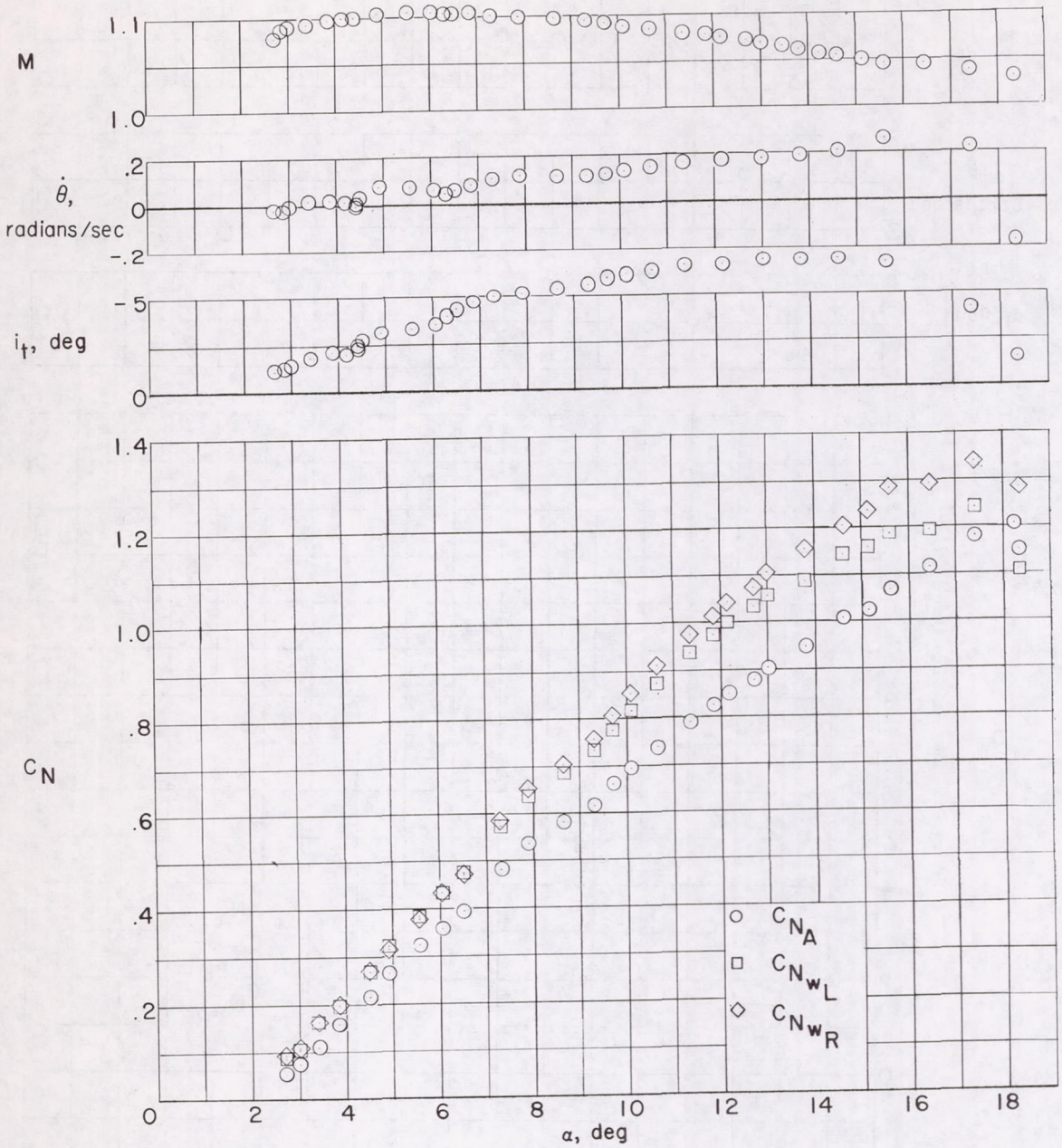
(c) $M \approx 0.89$; $h_p \approx 31{,}500$ feet.

Figure 3.- Continued.



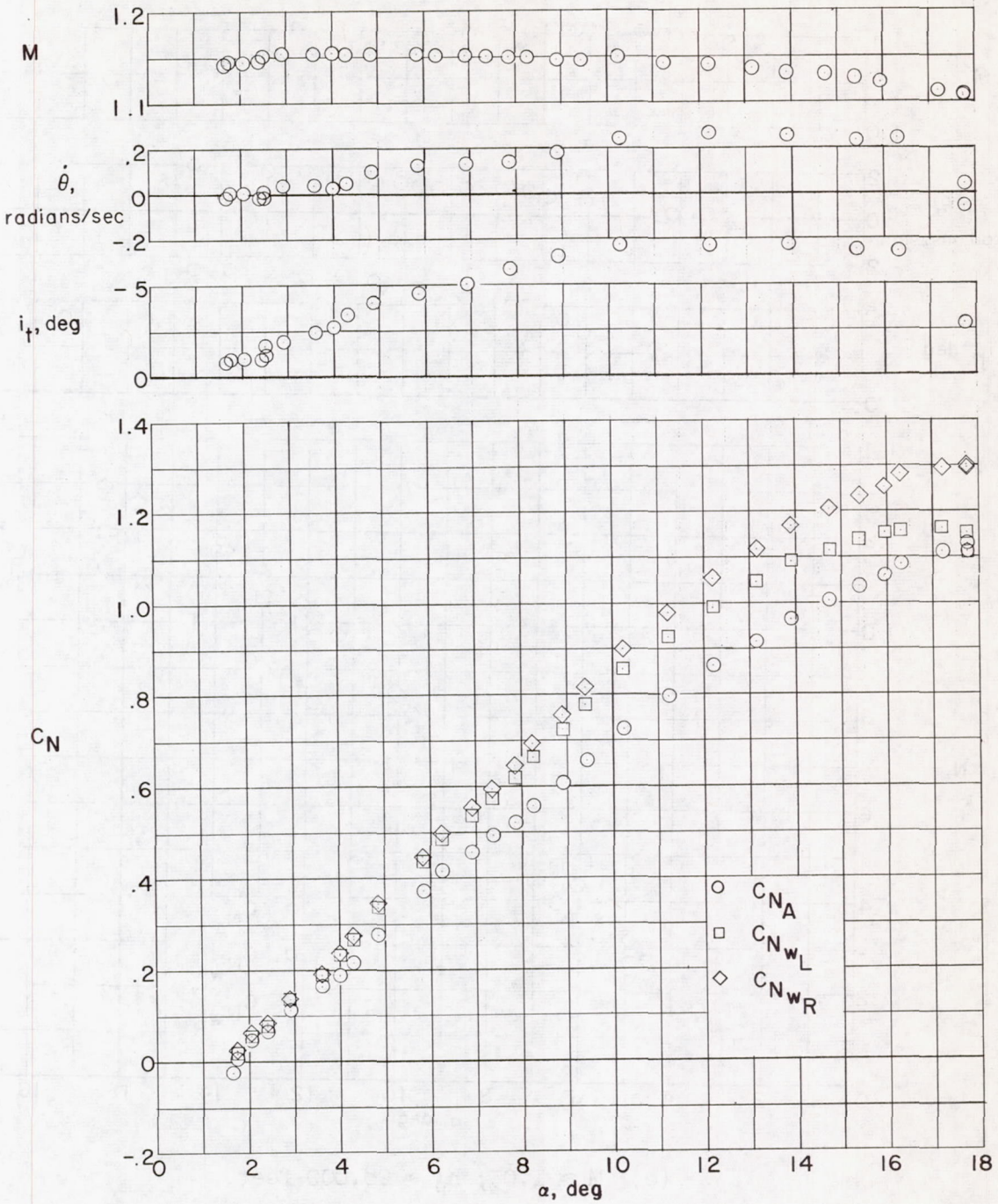
(d) $M \approx 0.93$; $h_p \approx 32{,}000$ feet.

Figure 3.- Continued.



(e) $M \approx 1.05$; $h_p \approx 28{,}000$ feet.

Figure 3.- Continued.



(f) $M \approx 1.10$; $h_p \approx 29{,}500$ feet.

Figure 3.- Concluded.

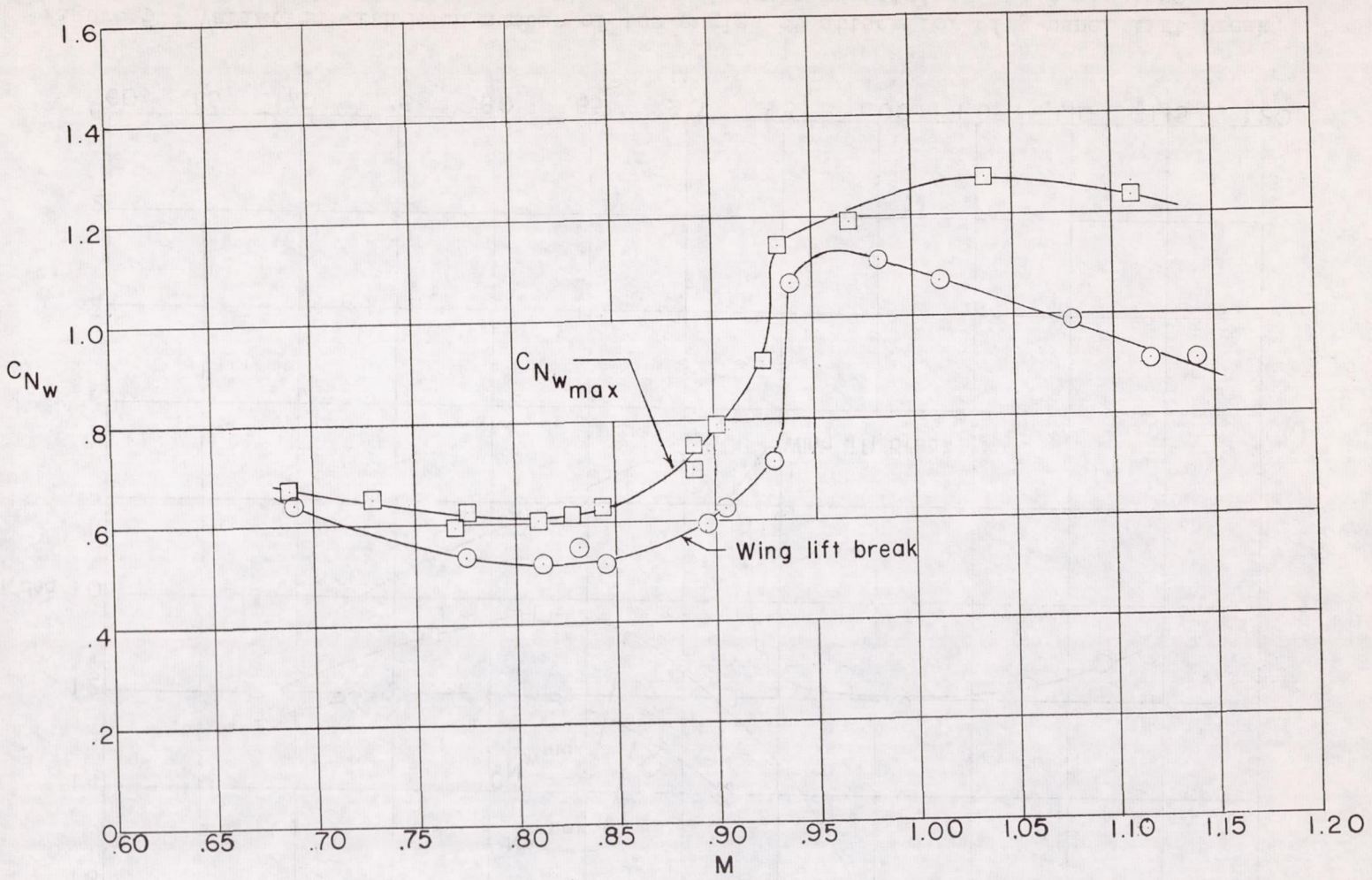


Figure 4.- Variation with Mach number of wing-panel lift break and wing-panel maximum normal-force coefficient. X-3 airplane.

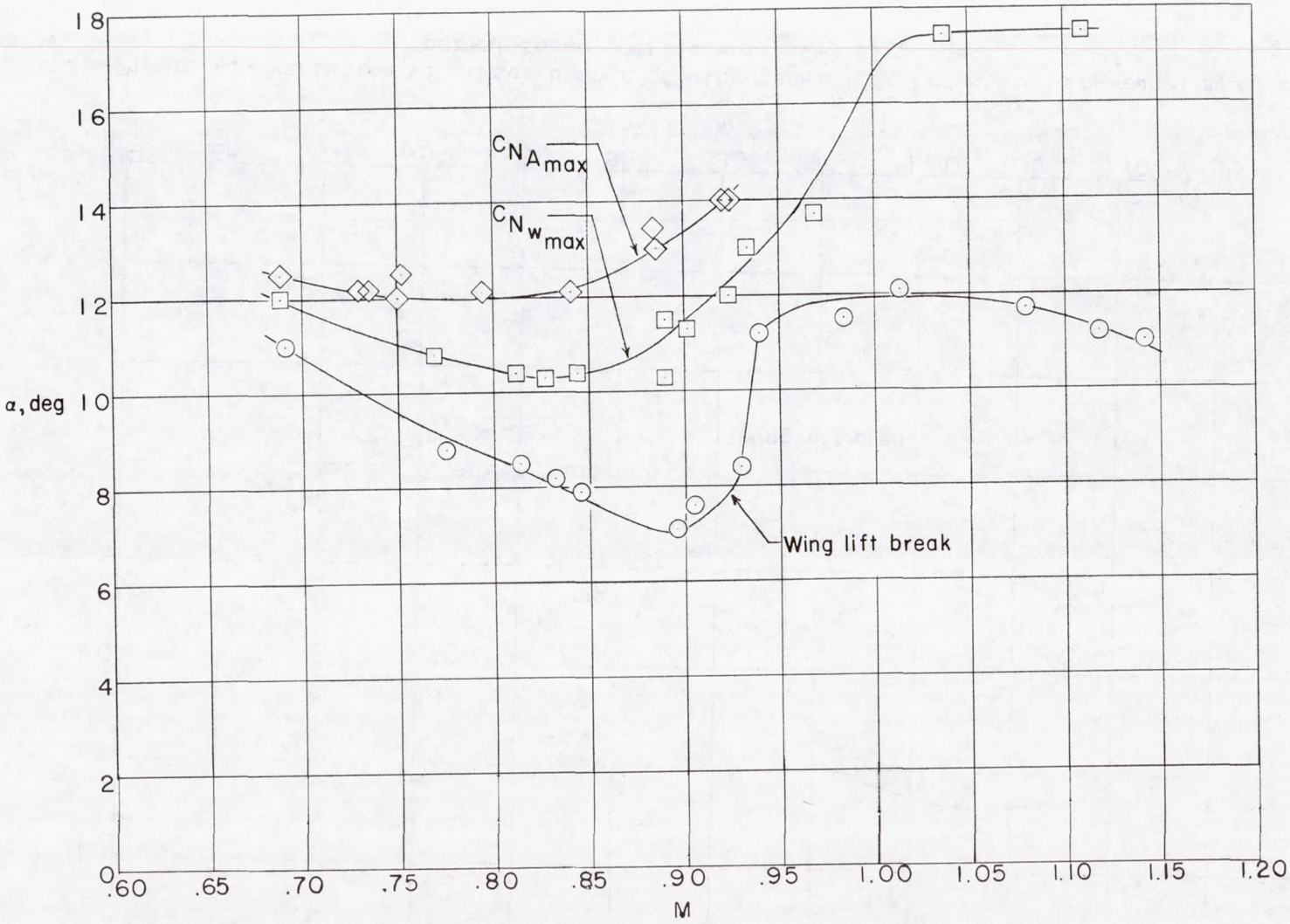


Figure 5.- Variation with Mach number of the angles of attack for wing-panel lift break, and wing-panel and airplane maximum normal-force coefficient. X-3 airplane.

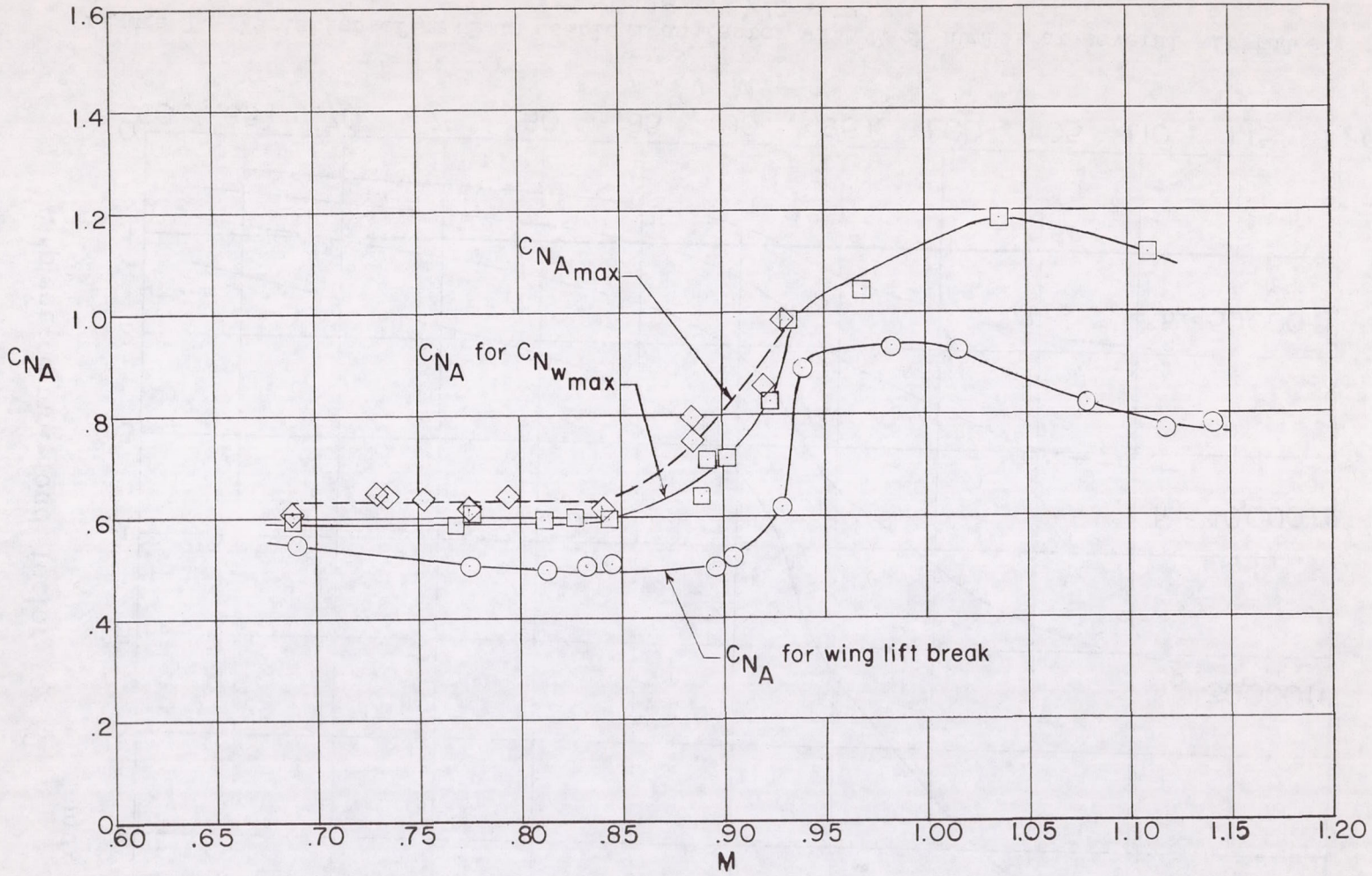


Figure 6.- Variation with Mach number of airplane normal-force coefficient for wing-panel lift break, wing-panel maximum normal-force coefficient, and airplane maximum normal-force coefficient. X-3 airplane.

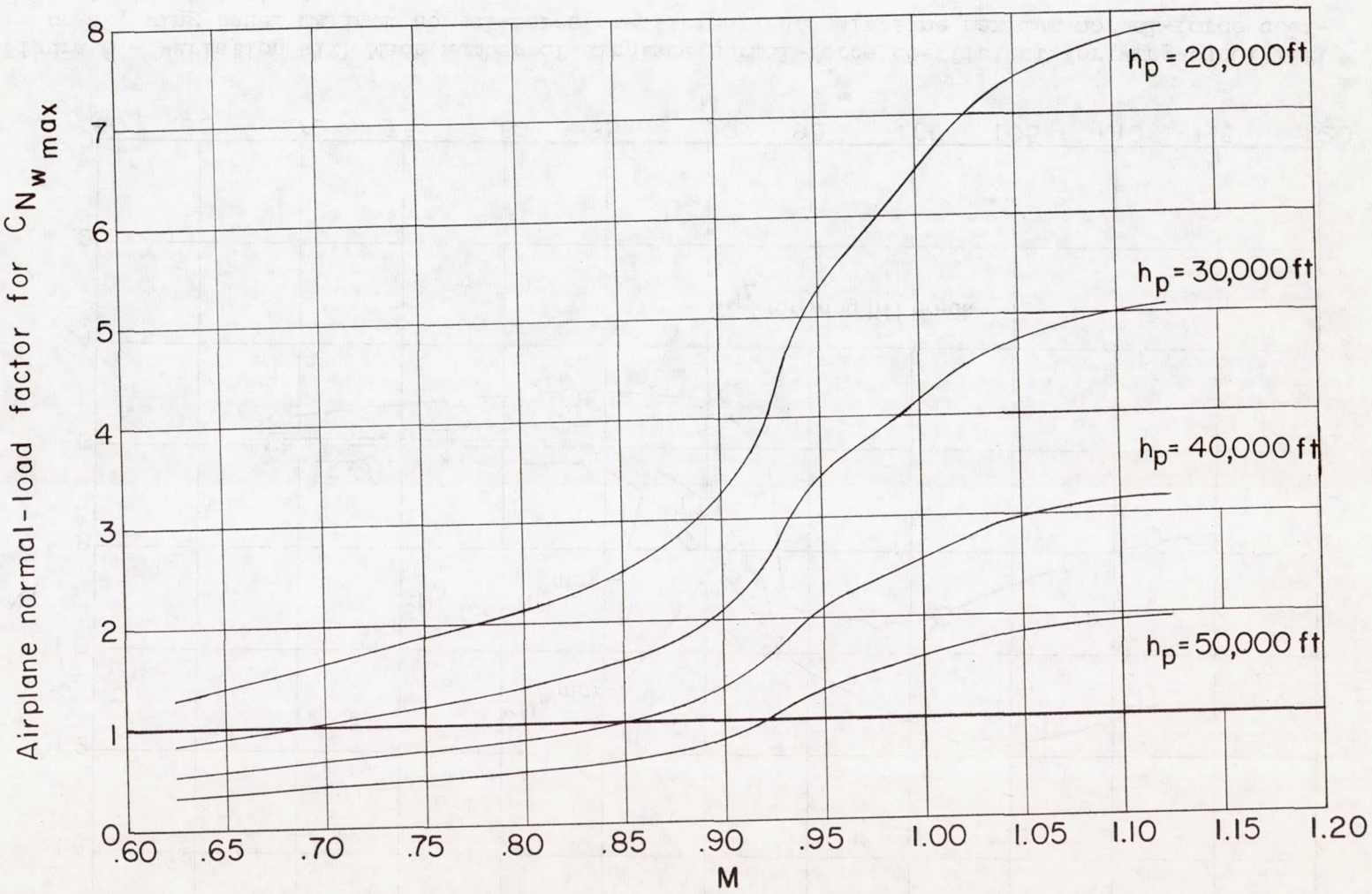
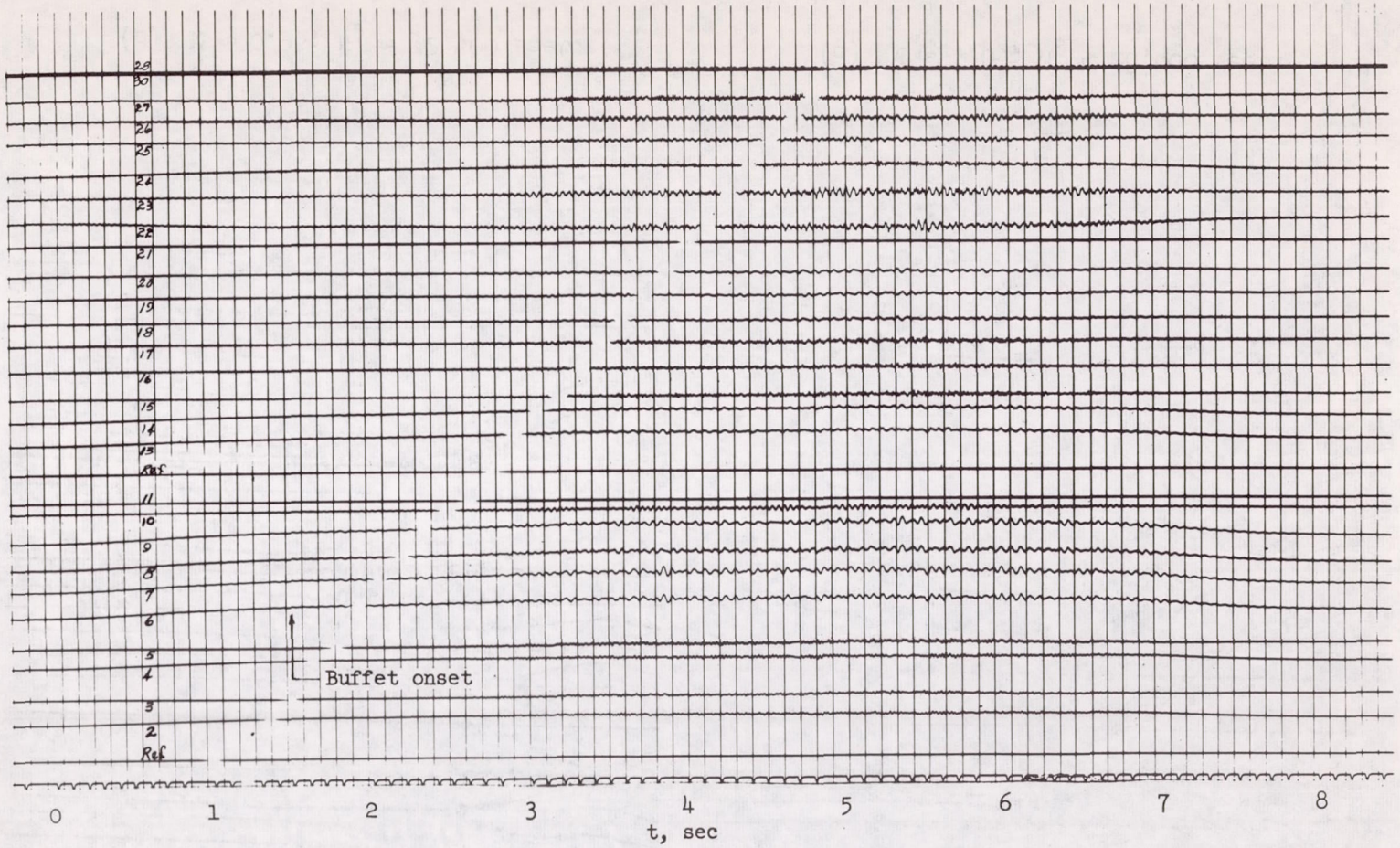
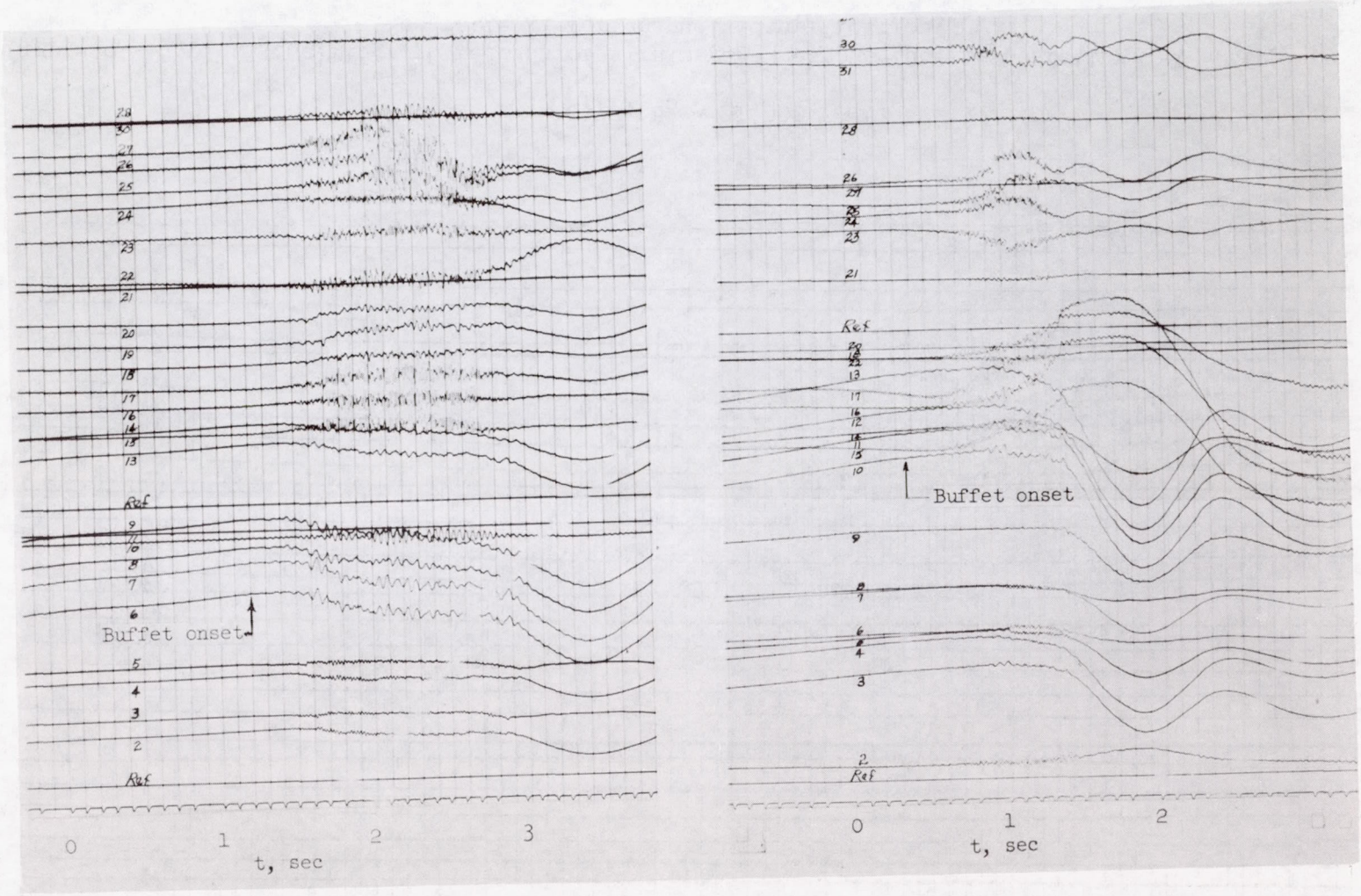


Figure 7.- Variation of maximum usable load factor with Mach number at several altitudes. X-3 airplane. W/S = 120.



(a) $M \approx 0.77$; $h_p \approx 31{,}500$ feet.

Figure 8.- Typical oscillograph records of strain-gage response during buffeting. X-3 airplane. (See table II for channel identification.)



(b) $M \approx 0.95$; $h_p \approx 32{,}500$ feet.

(c) $M \approx 1.05$; $h_p \approx 28{,}000$ feet.

Figure 8.- Concluded.

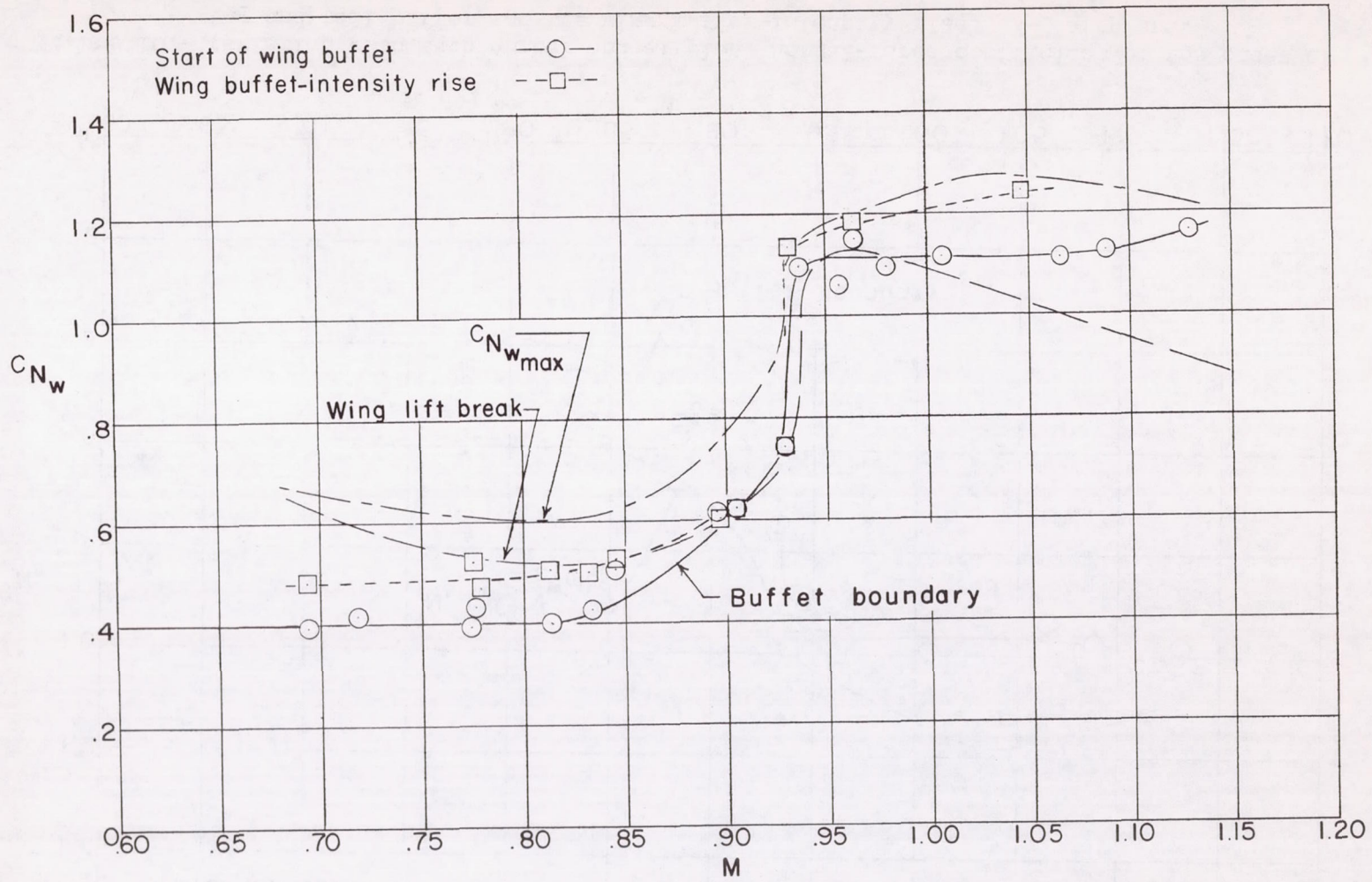


Figure 9.- Variation with Mach number and wing-panel normal-force coefficient of the wing buffet boundary and wing buffet-intensity-rise boundary. X-3 airplane.

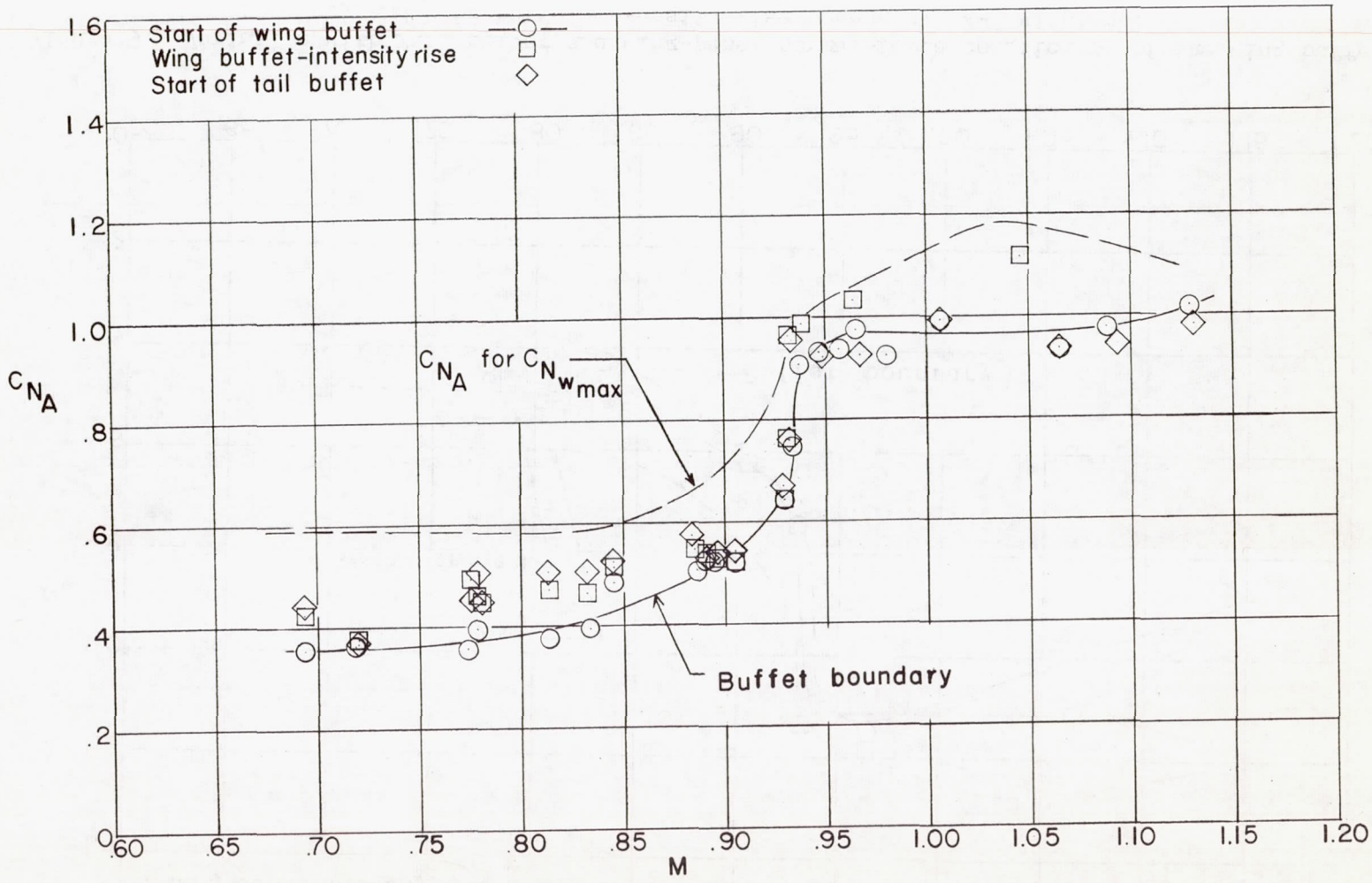


Figure 10.- Variation with Mach number and airplane normal-force coefficient of the onset of wing and tail buffet and the wing buffet-intensity rise. X-3 airplane.

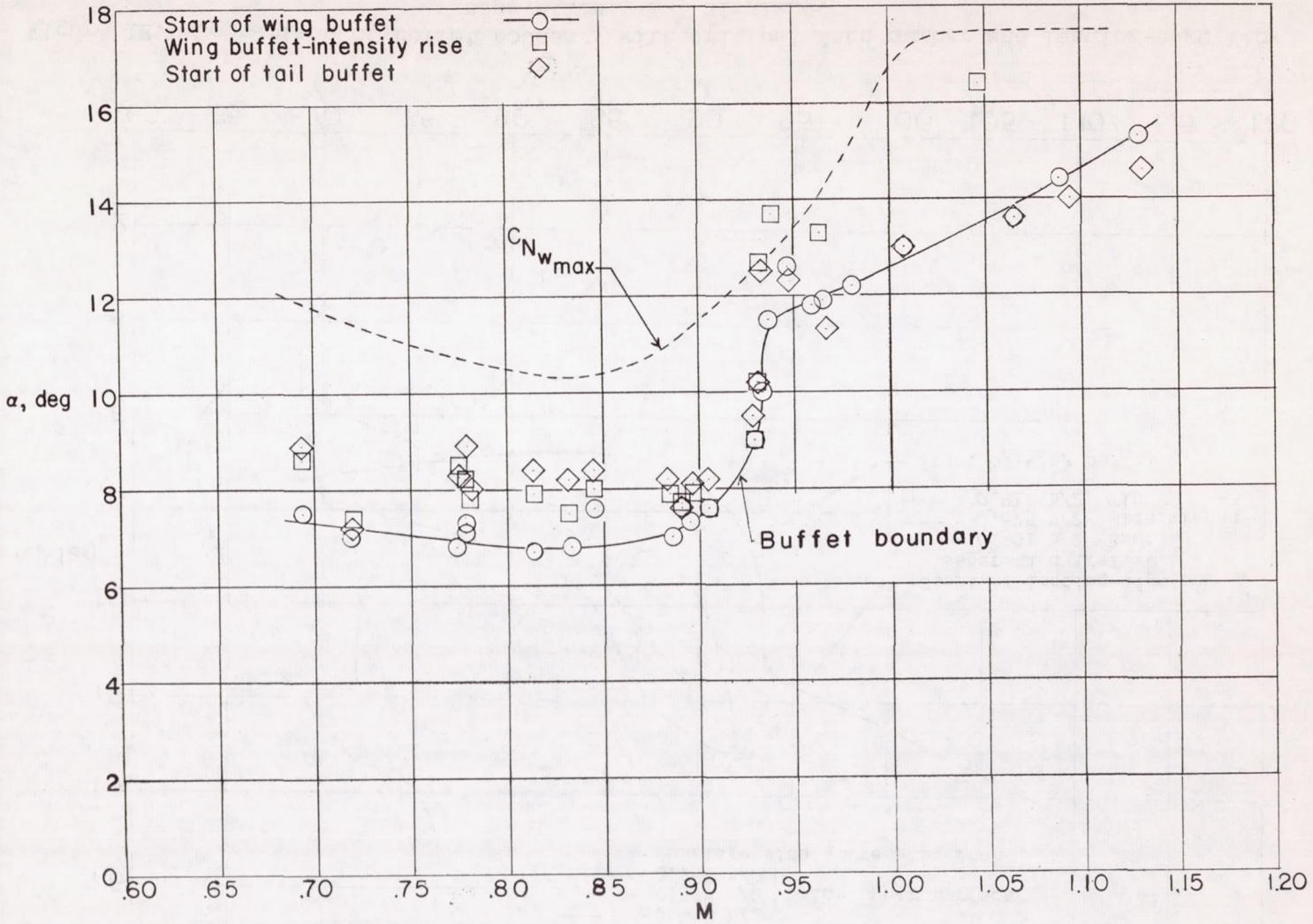


Figure 11.- Variation with Mach number and angle of attack of the onset of wing and tail buffet and the wing buffet-intensity rise. X-3 airplane.

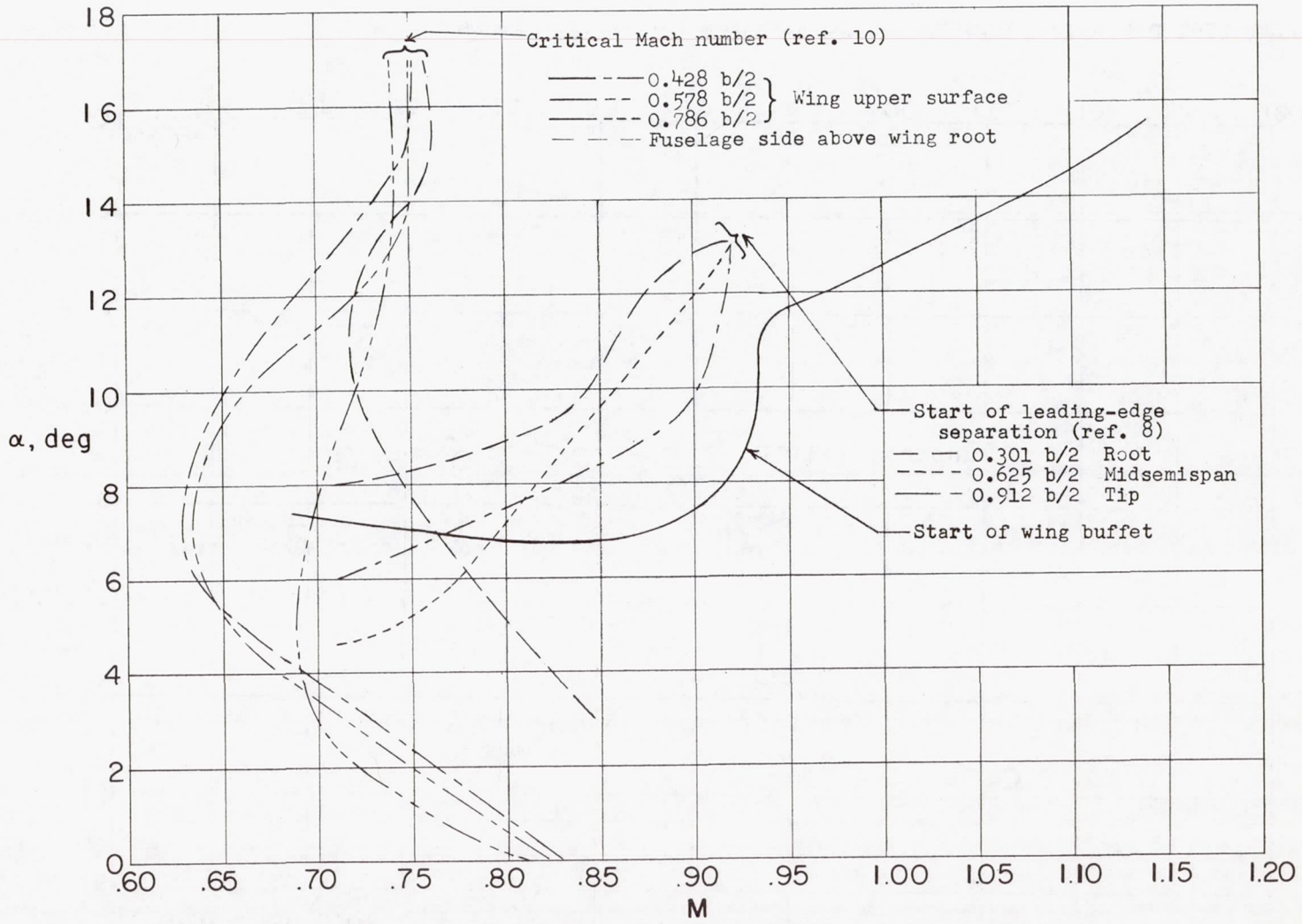


Figure 12.- Comparison of buffet boundary with critical Mach number and leading-edge flow separation. X-3 airplane.

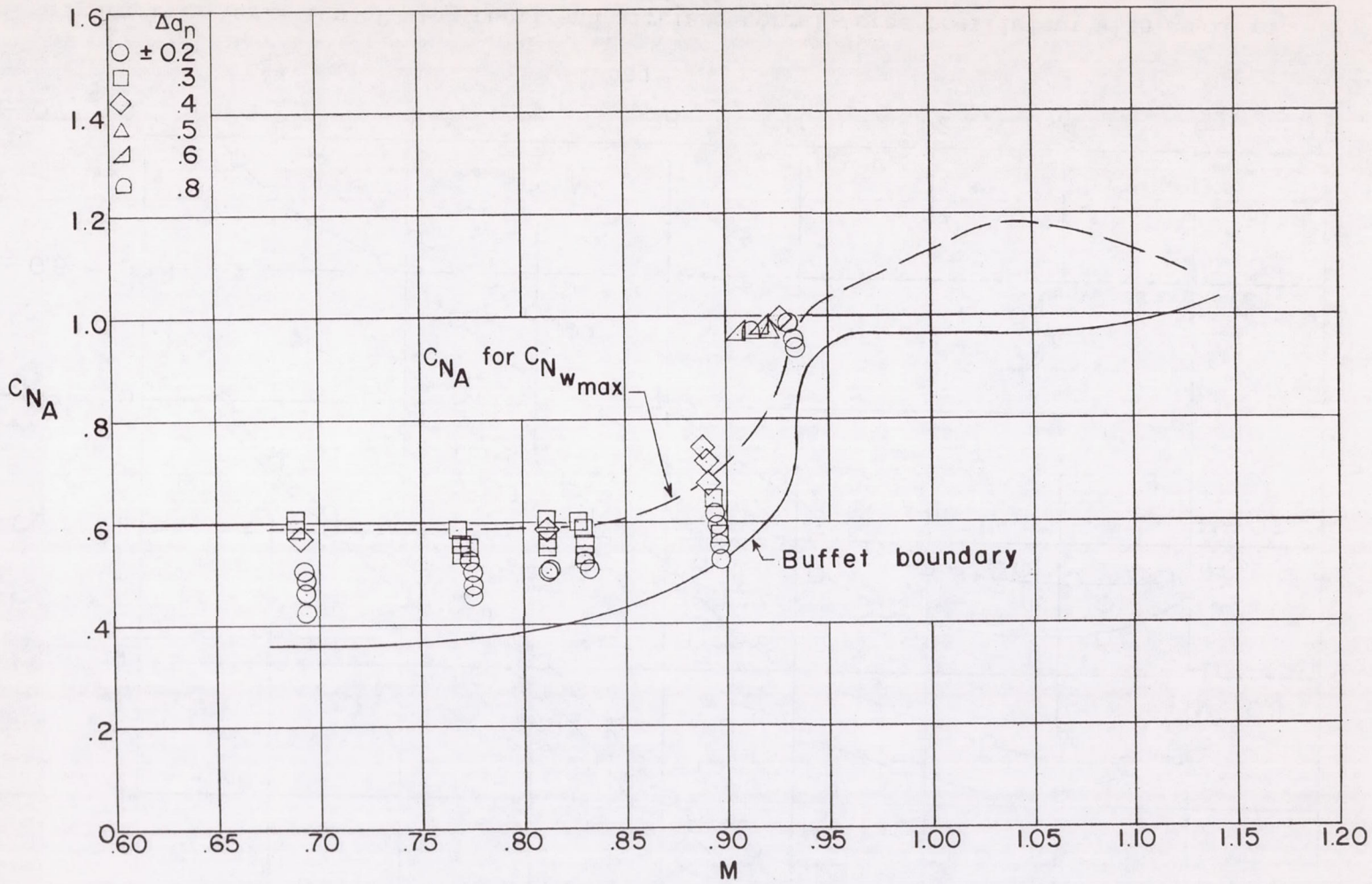


Figure 13.- Incremental acceleration amplitudes due to buffeting at airplane center of gravity; $h_p \approx 30{,}000$ feet. X-3 airplane.

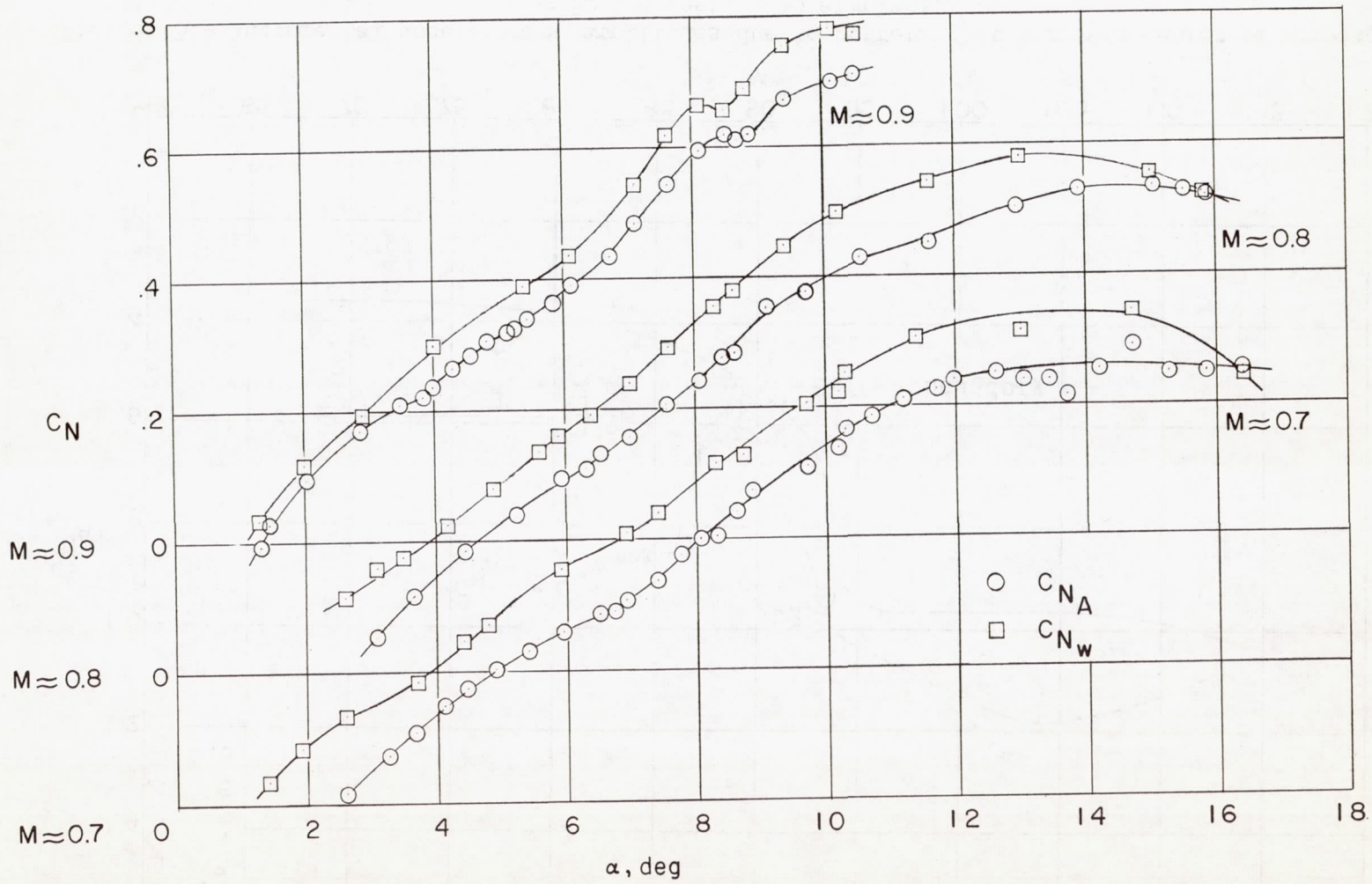


Figure 14.- Variation of wing panel and airplane normal-force coefficient with angle of attack. $\delta_{f_{le}} \approx 7^{\circ}$; X-3 airplane.

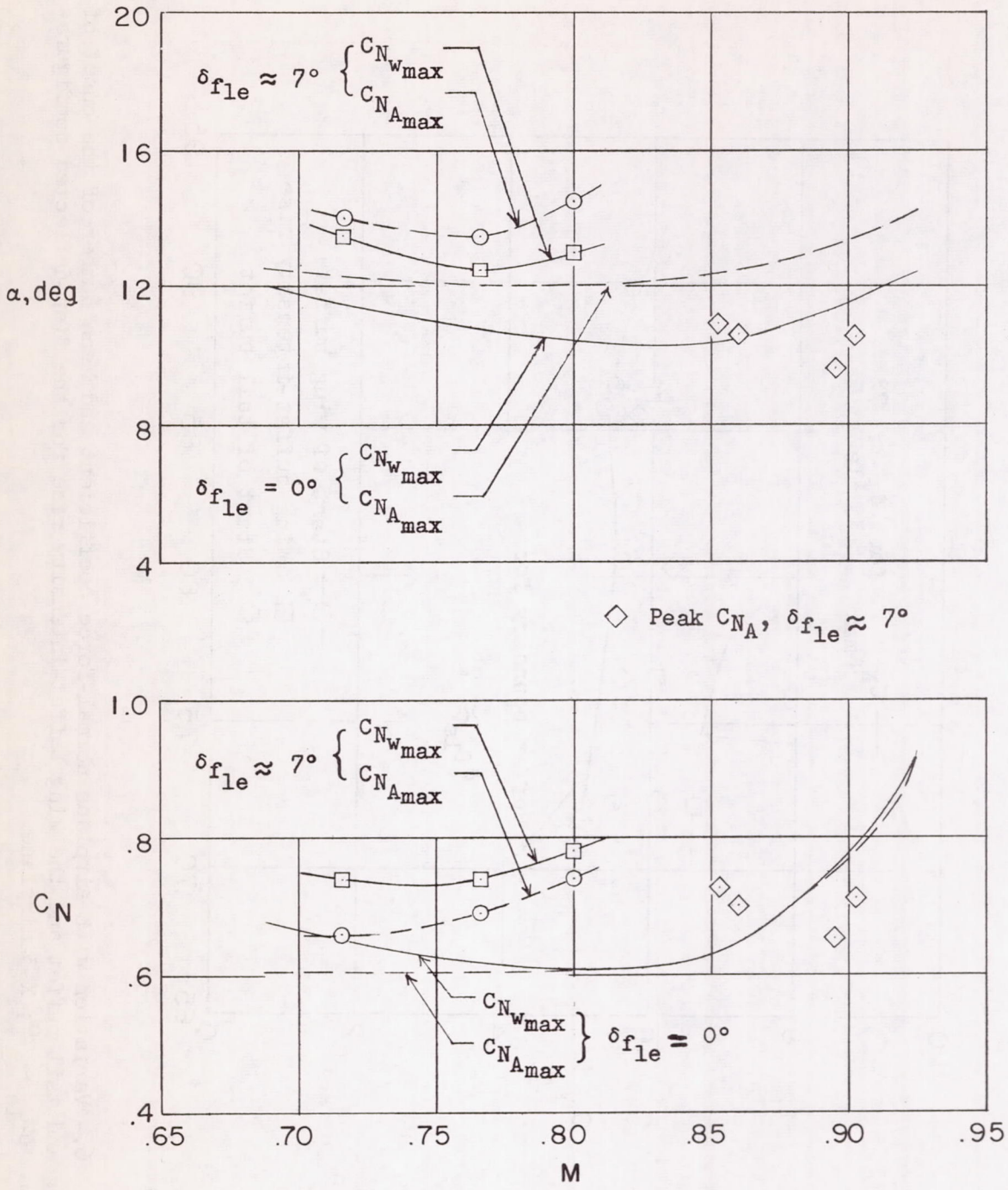


Figure 15.- Effect of the leading-edge-flap deflection on maximum lift. X-3 airplane.

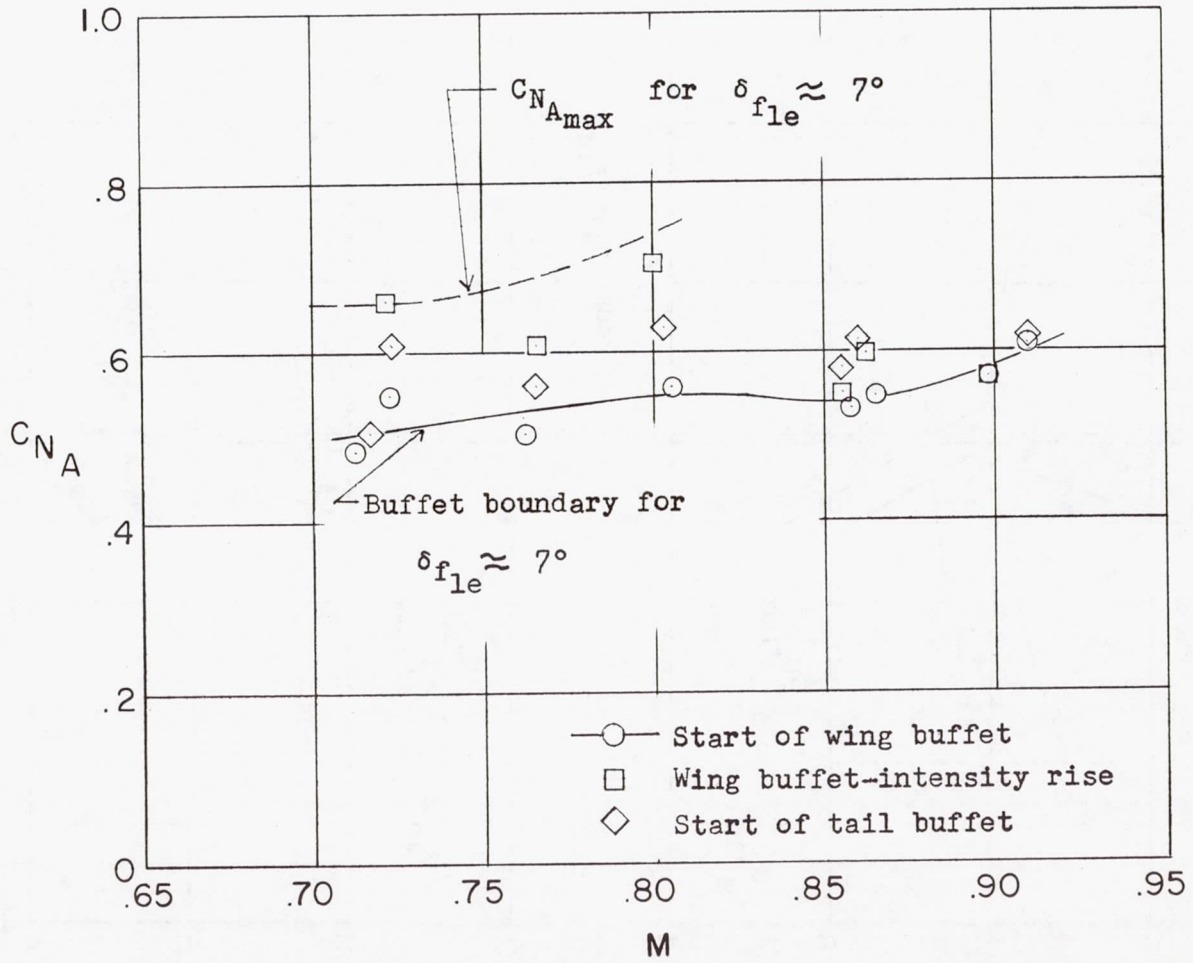


Figure 16.- Variation with airplane normal-force coefficient and Mach number of the onset of wing and tail buffet and the wing buffet-intensity rise for the flap-deflected configuration $\delta_{f_{le}} \approx 7°$; X-3 airplane.

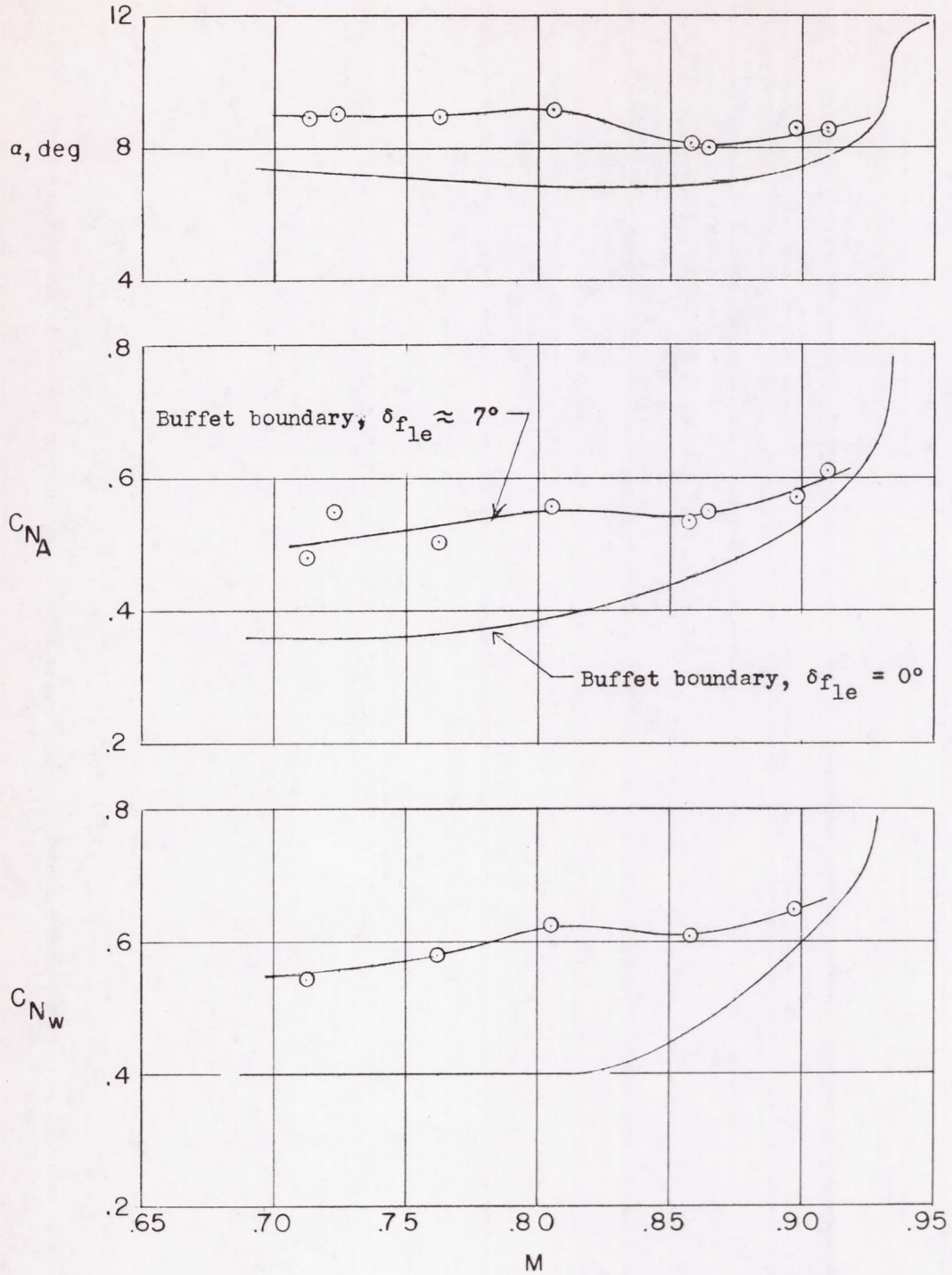


Figure 17.- Effect of a 7° deflection of wing leading-edge flaps on the start of buffeting.